

1
2 **Temperature and tropopause characteristics from**
3 **reanalyses data in the tropical tropopause layer**
4

5 Susann Tegtmeier^{1*}, James Anstey², Sean Davis³, Rossana Dragani⁴, Yayoi Harada⁵, Ioana
6 Ivanciu¹, Robin Pilch Kedzierski¹, Kirstin Krüger⁶, Bernard Legras⁷, Craig Long⁸, James S.
7 Wang⁹, Krzysztof Wargan^{10,11}, and Jonathon S. Wright¹²
8
9
10

11 ¹GEOMAR Helmholtz Centre for Ocean Research Kiel, 24105 Kiel, Germany

12 ^{*}now at Institute of Space and Atmospheric Studies, University of Saskatchewan, Saskatoon,
13 Canada

14 ²Canadian Centre for Climate Modelling and Analysis, ECCO, Victoria, Canada

15 ³Earth System Research Laboratory, National Oceanic and Atmospheric Administration,
16 Boulder, CO 80305, USA

17 ⁴European Centre for Medium-Range Weather Forecasts, Reading, RG2 9AX, UK

18 ⁵Japan Meteorological Agency, Tokyo, 100-8122, Japan

19 ⁶Section for Meteorology and Oceanography, Department of Geosciences, University of Oslo,
20 0315 Oslo, Norway

21 ⁷Laboratoire de Météorologie Dynamique, CNRS/PSL-ENS, Sorbonne University Ecole
22 Polytechnique, France

23 ⁸Climate Prediction Center, National Centers for Environmental Prediction, National Oceanic
24 and Atmospheric Administration, College Park, MD 20740, USA

25 ⁹Institute for Advanced Sustainability Studies, Potsdam, Germany

26 ¹⁰Science Systems and Applications, Inc., Lanham, MD 20706, USA

27 ¹¹Global Modeling and Assimilation Office, Code 610.1, NASA Goddard Space Flight
28 Center, Greenbelt, MD 20771, USA

29 ¹²Department of Earth System Science, Tsinghua University, Beijing, 100084, China
30
31
32
33
34
35
36
37

1 **Abstract**

2
3
4
5
6
7
8
9
10
11
12
13
14
15
16
17
18
19
20
21
22
23
24
25
26
27
28
29
30
31
32
33
34
35
36
37
38
39
40
41
42
43

The tropical tropopause layer (TTL) is the transition region between the well mixed, convective troposphere and the radiatively controlled stratosphere with air masses showing chemical and dynamical properties of both regions. The representation of the TTL in meteorological reanalysis data sets is important for studying the complex interactions of circulation, convection, trace gases, clouds and radiation. In this paper, we present the evaluation of climatological and long-term TTL temperature and tropopause characteristics in the reanalysis data sets ERA-Interim, ERA5, JRA-25, JRA-55, MERRA, MERRA-2, NCEP-NCAR (R1), and CFSR. The evaluation has been performed as part of the SPARC (Stratosphere– troposphere Processes and their Role in Climate) Reanalysis Intercomparison Project (S-RIP).

The most recent atmospheric reanalysis data sets (ERA-Interim, ERA5, JRA-55, MERRA-2, and CFSR) all provide realistic representations of the major characteristics of the temperature structure within the TTL. There is good agreement between reanalysis estimates of tropical mean temperatures and radio occultation data, with relatively small cold biases for most data sets. Temperatures at the cold point and lapse rate tropopause levels, on the other hand, show warm biases in reanalyses when compared to observations. This tropopause-level warm bias is related to the vertical resolution of the reanalysis data, with the smallest bias found for data sets with the highest vertical resolution around the tropopause. Differences of the cold point temperature maximise over equatorial Africa, related to Kelvin wave activity and associated disturbances in TTL temperatures.

Interannual variability in reanalysis temperatures is best constrained in the upper TTL, with larger differences at levels below the cold point. The reanalyses reproduce the temperature responses to major dynamical and radiative signals such as volcanic eruptions and the QBO. Long-term reanalysis trends in temperature in the upper TTL show good agreement with trends derived from adjusted radiosonde data sets indicating significant stratospheric cooling of around -0.5 to -1 K/decade. At 100 hPa and the cold point, most of the reanalyses suggest small but significant cooling trends of -0.3 to -0.6 K/decade that are statistically consistent with trends based on the adjusted radiosonde data sets.

Advances of the reanalysis and observational systems over the last decades have led to a clear improvement of the TTL reanalyses products over time. Biases of the temperature profiles and differences in interannual variability clearly decreased in 2006, when densely sampled radio occultation data started being assimilated by the reanalyses. While there is an overall good agreement, different reanalyses offer different advantages in the TTL such as realistic profile and cold point temperature, continuous time series or a realistic representation of signals of interannual variability. Their use in model simulations and in comparisons with climate model output should be tailored to their specific strengths and weaknesses.

1 **1. Introduction**

2
3 The tropical tropopause layer (TTL) is the transition region between the well-mixed, convective
4 troposphere and the radiatively-controlled stratosphere. The vertical range of the TTL extends
5 from the region of strong convective outflow near 12-14 km to the highest altitudes reached by
6 convective overshooting events, around 18 km (Highwood and Hoskins, 1998; Folkins et al
7 1999; Fueglistaler et al., 2009; Randel and Jensen, 2013). Air masses in the TTL show
8 dynamical and chemical properties of both the troposphere and the stratosphere, and are
9 controlled by numerous processes on a wide range of length and time scales. Complex
10 interactions among circulation, convection, trace gases, clouds and radiation in the TTL make
11 this region a key player in radiative forcing and chemistry-climate coupling. As the TTL is the
12 main gateway for air entering the stratosphere, stratospheric chemistry and composition, and
13 especially the abundances of ozone, water vapour and aerosols, are strongly impacted by the
14 properties of air near the tropical tropopause (e.g., Mote et al., 1996; Holton and Gettelman,
15 2001; Fueglistaler et al., 2011).

16
17 The tropopause is the most important physical boundary within the TTL, serving to separate
18 the turbulent, moist troposphere from the stable, dry stratosphere. The position of the
19 tropopause is determined by the thermal properties of the TTL, as a negative, tropospheric
20 vertical temperature gradient changes into a positive stratospheric temperature gradient. The
21 role of the tropopause as a physical boundary is evident not only from the vertical temperature
22 structure, but also from the distributions of atmospheric trace gases and clouds (Pan and
23 Munchak, 2011; Pan et al., 2018).

24
25 In the tropics, two definitions of the tropopause are widely used: one based on the cold point
26 and one based on the characteristics of the lapse rate. The cold point tropopause is defined as
27 the level at which the vertical temperature profile reaches its minimum (Highwood and Hoskins,
28 1998) and air parcels en route from the troposphere to the stratosphere encounter the lowest
29 temperatures. Final dehydration typically occurs at these lowest temperatures, so that the cold
30 point tropopause effectively controls the overall water vapour content of the lower stratosphere
31 (Randel et al., 2004a) and explains its variability (Fueglistaler et al., 2009). While the cold point
32 tropopause is an important boundary in the tropics where upwelling predominates, this
33 definition of the tropopause is irrelevant for water vapor transport into the stratosphere at higher
34 latitudes. The lapse rate tropopause, on the other hand, offers a globally-applicable definition
35 of the tropopause, marking a vertical discontinuity in the static stability. The lapse rate
36 tropopause is defined as the lowest level at which the lapse rate decreases to 2 K km^{-1} or less,
37 provided that the average lapse rate between this level and all higher levels within 2 km does
38 not exceed 2 K km^{-1} (World Meteorological Organization, 1957). The tropical lapse rate
39 tropopause is typically $\sim 0.5 \text{ km}$ ($\sim 7 \text{ hPa}$) lower and $\sim 1 \text{ K}$ warmer than the cold point tropopause
40 (Seidel et al., 2001).

41
42 Over recent decades, the thermal characteristics of the TTL and tropopause have been obtained
43 from tropical radiosonde and Global Navigation Satellite System - Radio Occultation (GNSS-
44 RO) upper air measurements. Radiosonde profiles offer temperature, wind and air pressure data
45 at a high vertical resolution. However, climate records based on radiosonde data often suffer

1 from spatial inhomogeneities or time-varying biases due to changes in instruments and
2 measurement practices (Seidel and Randel, 2006; Wang et al., 2012). Climate records from
3 radio occultation data offer much better spatial coverage and density, but are only available
4 starting from 2002. As a result, studies of long-term variability and trends in TTL and
5 tropopause properties have also used reanalysis data (e.g., Santer et al., 2003; Gettelman et al.,
6 2010, Xie et al., 2014).

7
8 Meteorological reanalysis data sets are widely used in scientific studies of atmospheric
9 processes and variability, either as initial conditions for historical model runs or in comparisons
10 with climate model output. Often, they are utilized as “stand-ins” for observations, when the
11 available measurements lack the spatial or temporal coverage needed. Each atmospheric
12 reanalysis system consists of a fixed global forecast model and assimilation scheme. The system
13 combines short-range forecasts of the atmospheric state with available observations to produce
14 best-guess, consistent estimates of atmospheric variables such as temperatures and winds.
15 Spurious changes in the reanalysis fields can arise from changes in the quality and quantity of
16 the observations used as input data, which complicates the analysis of variability and trends.
17 Further discontinuities in reanalysis-based time series can originate from the joining together
18 of distinct execution streams (Fujiwara et al., 2017).

19
20 Among the various TTL characteristics such as composition, radiation budgets and cloud
21 properties, the vertical temperature structure and the position and temperature of the cold point
22 are of particular importance for transport and composition studies. Many off-line chemistry-
23 transport models or Lagrangian particle dispersion models are driven by reanalysis data sets
24 (e.g., Chipperfield, 1999; Krüger et al., 2009; Schoeberl et al, 2012; Tao et al., 2019). Their
25 representation of the cold point determines how realistically such models simulate dehydration
26 and stratospheric entrainment processes. Process studies of TTL dynamics such as equatorial
27 wave variability are also often based on the TTL temperature structure in reanalysis data sets
28 (e.g., Fujiwara et al., 2012). Finally, reanalysis cold point temperature and height have been
29 used in the past for comparison to model results and in investigations of long-term changes
30 (e.g., Gettelman et al., 2010). Information on the quality and biases of TTL temperature and
31 tropopause data are important for all above listed studies of transport, composition, dynamics
32 and long-term changes of the TTL.

33
34 A comparison of the reanalysis products available at the end of the 1990s (including ERA-15,
35 ERA-40 and NCEP-NCAR R1) with other climatological datasets showed notable differences
36 in temperatures near the tropical tropopause (Randel et al., 2004b). While the ECWMF
37 reanalyses agreed relatively well with radiosonde observations at 100 hPa, NCEP-NCAR R1
38 showed a warm bias of up to 3 K, probably resulting from low vertical resolution and the use
39 of poorly-resolved satellite temperature retrievals (Fujiwara et al., 2017). Comparisons of
40 winter temperatures at 100 hPa between more recent reanalyses, such as MERRA, NCEP CFSR
41 and ERA-Interim, and Singapore radiosonde observations show better agreement, with
42 reanalyses generally 1-2 K too cold at this level (Schoeberl et al, 2012). While many studies
43 have highlighted the characteristics of individual reanalysis data sets, a comprehensive
44 intercomparison of the TTL among all major atmospheric reanalyses is currently missing.

1 Here, we investigate whether the reanalysis data sets ERA-Interim, ERA5, JRA-25, JRA-55,
2 MERRA, MERRA-2, NCEP-NCAR (R1), and CFSR reproduce key characteristics of the
3 temperature and tropopause in the TTL. This work has been conducted as part of the SPARC
4 (Stratosphere–troposphere Processes and their Role in Climate) Reanalysis Intercomparison
5 Project (S-RIP) (Fujiwara et al., 2017) and presents some of the key findings from the S-RIP
6 report Chapter 8 on the TTL. Climatologies of the tropical cold point and lapse rate tropopause
7 as derived from modern reanalysis data sets are compared to high-resolution radio occultation
8 data (Section 3). We also investigate temporal variability and long-term changes in tropopause
9 levels and temperature within the TTL (Section 4). The observational and reanalysis data sets
10 used in the evaluation are introduced in Section 2, and a discussion and summary of the results
11 are provided in Section 5.

12

13 **2 Data and methods**

14

15 **2.1 Observational data sets**

16

17 Observations of the TTL temperatures are available from tropical radiosonde stations.
18 However, climate records of radiosonde temperature, height and pressure data often suffer from
19 inhomogeneities or time-varying biases due to changes in instruments or measurement practices
20 (Seidel and Randel, 2006). Adjusted radiosonde temperature data sets at 100 hPa, 70 hPa and
21 corresponding trends at the cold point have been created by removing such inhomogeneities
22 (Wang et al., 2012, and references therein). In this chapter, we use the four independently
23 adjusted radiosonde data sets RATPAC (Free et al., 2005), RAOBCORE (Haimberger, 2007),
24 RICH (Haimberger et al., 2012) and HadAT (Thorne et al., 2005) for evaluations at 70 and 100
25 hPa. The interannual anomalies at 70 hPa are shown only for RAOBCORE to improve the
26 clarity of the figure, but all data sets are discussed in the text. For trends at 70 and 100 hPa, we
27 show the smallest and largest trends derived from the four adjusted radiosonde data sets as
28 reported by Wang et al. (2012) and consider their range (including error bars) as the
29 observational uncertainty range.

30 Evaluations of the interannual anomalies of cold point temperature, height and pressure are
31 based on the unadjusted, quality-controlled radiosonde data set IGRA (Durre et al., 2006) as
32 temperature adjustments can change the location of the cold point in a profile. The trend of cold
33 point temperature cannot be derived from the unadjusted IGRA data set due to inhomogeneities
34 or time-varying biases caused by changes in instruments and measurement practices (see Wang
35 et al., 2012 for a detailed discussion). Instead we use adjusted cold points derived from the
36 adjusted radiosonde data sets discussed above.

37 Since 2002, high-resolution temperature and pressure data in the TTL are also available from
38 satellite retrievals based on the GNSS-RO technique. Recent studies have demonstrated good
39 agreement between GNSS-RO and radiosonde temperature profiles (e.g. Anthes et al., 2008;
40 Ho et al., 2017). We use a monthly mean zonal mean data set constructed from measurements
41 collected by the Challenging Minisat Payload (CHAMP, Wickert et al., 2001), Gravity
42 Recovery and Climate Experiment (GRACE, Beyerle et al., 2005), Constellation Observing
43 System for Meteorology, Ionosphere, and Climate (COSMIC, Anthes et al., 2008), Metop-A
44 (von Engel et al., 2011), Metop-B, Satélite de Aplicaciones Científicas-C/Scientific

1 Application Satellite-C (SAC-C, Hajj et al., 2004), and TerraSAR-X (Beyerle et al., 2011)
2 missions. All data are re-processed or post-processed occultation profiles with moisture
3 information ('wetPrf' product) as provided by the COSMIC Data Analysis and Archive Center
4 (CDAAC, <https://cdaac-www.cosmic.ucar.edu/cdaac/products.html>). The GNSS-RO 'wetPrf'
5 temperature profiles from CDAAC are provided on a 100-m vertical grid from the surface to
6 40 km altitude. The effective physical resolution is variable, ranging from ~1 km in regions of
7 constant stratification down to 100-200m where the biggest stratification gradients occur e.g.
8 at the top of the boundary layer or at a very sharp tropopause (Kursinski et al., 1997; Gorbunov
9 et al., 2004), most often being somewhere in between. The observational temperature records
10 at reanalysis model levels in the TTL region have been determined by interpolating each GNSS-
11 RO temperature profile to the reanalysis model levels with the barometric formula, taking into
12 account the lapse rate between levels. For each profile, the cold point and lapse rate tropopause
13 characteristics were identified based on the cold point and WMO criteria, respectively. Zonal
14 and long-term averages of the tropopause metrics and temperatures at model levels are
15 calculated by averaging over all grid points and represent the final step of data processing.

16 We also use a daily data set of cold point temperatures obtained from all GNSS-RO missions,
17 gridded on a $5^\circ \times 5^\circ$ grid between 30°N and 30°S . For each 5° wide latitude band, we apply a
18 two-dimensional fast Fourier transform to detect Kelvin wave anomalies for planetary
19 wavenumbers 1–15, periods of 4–30 days and equivalent depths of 6–600 following the
20 theoretical dispersion curves for Kelvin waves as in Wheeler and Kiladis (1999). We allow a
21 wider range of equivalent depths, since it has been shown that Kelvin waves tend to propagate
22 faster around the tropical tropopause than they do in the troposphere (Kim and Son, 2012). The
23 filtered anomalies represent cold point temperature variability that propagates in the same
24 wavenumber-frequency domain as Kelvin waves, i.e. when the temperature is modulated by
25 Kelvin waves present around the tropopause. The spatial variance of the filtered signals is used
26 to calculate a monthly index as a measure of the amount of Kelvin wave activity in the TTL.
27 The index is calculated as the 1σ standard deviation over the filtered anomalies at all spatial
28 grid points. Time periods of enhanced Kelvin wave activity are defined as the months when the
29 index is larger than the long-term mean plus the 1σ standard deviation of the whole time series.
30 Based on this definition, we determined 20% of all months to be characterized by enhanced
31 Kelvin wave activity.

32

33 **2.2 Reanalysis data sets**

34

35 We evaluate eight “full-input” reanalyses, where a full-input reanalysis is defined as a systems
36 that assimilate surface and upper-air conventional and satellite data. In this paper, we focus on
37 the European Centre for Medium-Range Weather Forecasts (ECMWF) Interim Reanalysis
38 (ERA-Interim; Dee et al., 2011), the forthcoming reanalysis developed by ECMWF (ERA5;
39 Hersbach et al., 2018), the Japanese 25-year Reanalysis (JRA-25; Onogi et al., 2007), the
40 Japanese 55-year Reanalysis (JRA-55; Kobayashi et al., 2015), the Modern Era Retrospective-
41 Analysis for Research (MERRA; Rienecker et al., 2011), the MERRA-2 (Gelaro et al., 2017),
42 the National Centers for Environmental Prediction (NCEP) - National Center for Atmospheric
43 Research (NCAR) Reanalysis 1 (NCEP-NCAR Reanalysis 1; Kistler et al., 2001; referred to

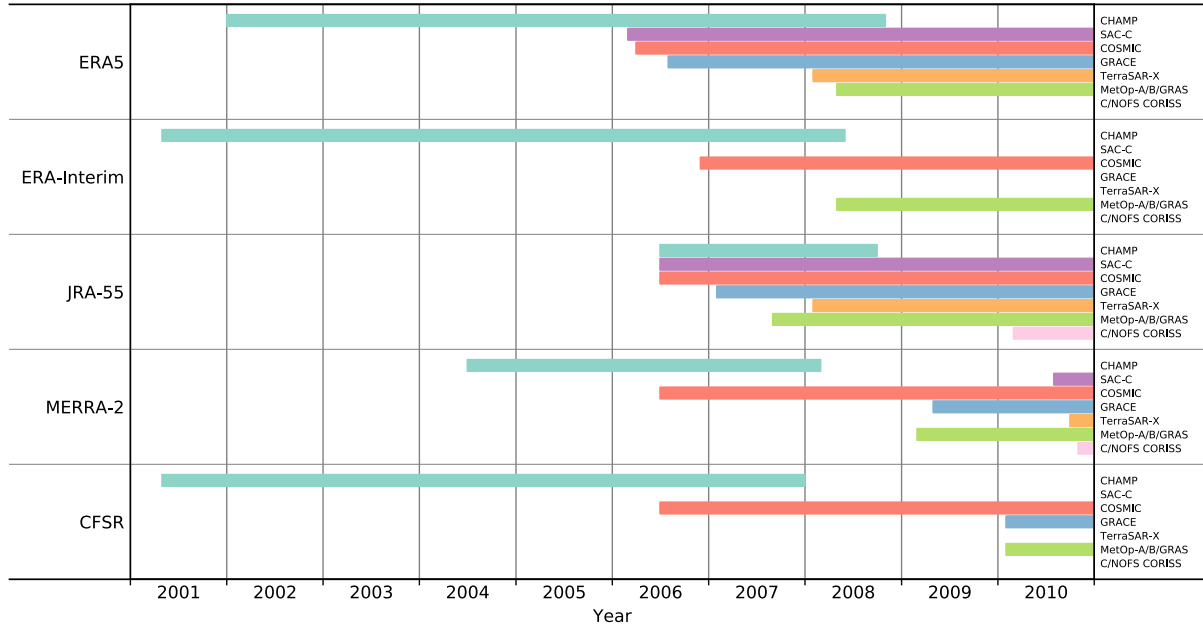
1 hereafter as R1), and the Global Forecast System of the NCEP Reanalysis (CFSR; Saha et al.,
2 2010). We limit our analyses to the S-RIP core intercomparison period 1980–2010. Due to
3 availability at the time of the evaluations, ERA5 is only evaluated over 2002–2010. Details of
4 each reanalysis, including model characteristics, physical parameterizations, assimilated
5 observations, execution streams, and assimilation strategies have been summarized by Fujiwara
6 et al. (2017).

7 Global temperature fields in the reanalysis data sets are constrained by assimilating
8 conventional (surface and balloon), aircraft, and satellite observations. The most important
9 sources of assimilated data for stratospheric temperatures are the microwave and infrared
10 satellite sounders of the TOVS suite (1979–2006) and the ATOVS suite (1998–present). All of
11 the above reanalysis systems assimilate microwave and infrared radiances from these
12 instruments, except for NCEP-NCAR R1 which assimilates temperature retrievals instead.
13 Measurements from the ATOVS suite, which has a higher number of channels compared to
14 TOVS, have been assimilated from about 1998, although the exact start dates differ among the
15 reanalyses. The introduction of ATOVS considerably improved the vertical resolution of the
16 assimilated data. Some of the reanalyses (ERA-Interim, ERA5, MERRA, MERRA-2, and
17 CFSR) also assimilate radiances from the hyperspectral infrared sounders AIRS (2002–
18 present), IASI (2008–present), and/or CrIS (2012–present), although the latter was not available
19 for assimilation during the intercomparison period considered here. Because radiance biases
20 associated with instrument changes, inaccurate calibration offsets, orbital drifts or long-term
21 CO₂ changes can cause unwanted biases in the resulting reanalysis temperature fields (e.g.
22 Rienecker et al., 2011), a variational bias correction scheme is used during the data assimilation
23 procedure to remove or minimize any radiance biases. This ensures that any temperature
24 changes introduced by the circumstances outlined above are kept small, which is important
25 when looking for long term changes.

26 All full-input reanalyses assimilate upper-air temperature observations from radiosondes which
27 are available at a very high vertical resolution. Systematic errors in radiosonde profiles caused
28 by effects of solar radiative heating on the temperature sensor (Nash et al., 2011) have typically
29 been corrected either onsite or at the reanalysis centre before assimilation (Fujiwara et al.,
30 2017). In order to avoid discontinuities or inconsistencies in temperature time series from
31 radiosondes, several reanalysis systems use homogenized temperature data sets such as
32 RAOBCORE (ERA-Interim, JRA-55, MERRA, MERRA-2) and RICH (ERA5). Earlier
33 reanalyses (ERA-40 and JRA-25) used simplified homogenization approaches that mostly
34 corrected for daily and seasonal variations. Although the detailed quality control procedures for
35 radiosonde and other conventional data imported from the global distribution network can vary
36 among the individual reanalyses, the conventional data archives are often shared among the
37 centres (see also Fujiwara et al., 2017).

38 Recent reanalysis systems have also included information from GNSS-RO instruments by
39 assimilating observations of the bending angle up to 30 km (Cucurull et al., 2013). Assimilating
40 these high vertical resolution data affects reanalysis temperature and provides an additional
41 ‘anchor’ for adaptive bias correction of satellite radiances. JRA-55 assimilates refractivity
42 profiles up to 30 km, which are functions of temperature, humidity, and pressure. For all recent
43 reanalyses, the advent of the COSMIC mission in 2006 significantly increased the number of
44 GNSS-RO profiles available for assimilation. Details of the various GNSS-RO data assimilated

1 by ERA5, ERA-Interim, JRA-55, MERRA-2 and CFSR up to the end of 2010 are listed in
 2 **Table 1**. In addition to the GNSS-RO data sets discussed in section 2.1, C/NOFS-CORISS
 3 (Communications/Navigation Outage Forecasting System Occultation Receiver for
 4 Ionospheric Sensing and Specification) is assimilated by some of the reanalyses.
 5

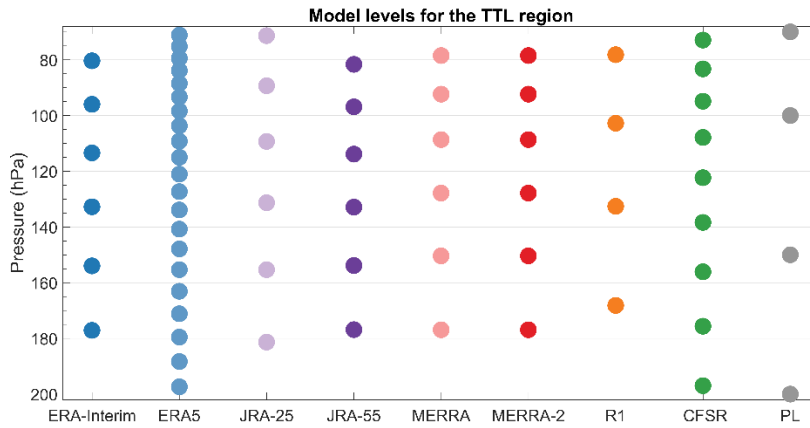


6
 7
 8 **Table 1.** List of GNSS-RO data assimilated by the reanalysis systems with starting dates prior to the end
 9 of 2010.

10
 11 Among the observational data sets, radiosonde and GNSS-RO data are our best source of
 12 information about the TTL. While the reanalyses assimilate different versions of these data, it
 13 is not automatic that they reproduce the data within their uncertainty ~~exactly~~. For instance,
 14 discrepancies exist between reanalysis stratospheric temperatures and those derived from their
 15 radiance input data (Long et al., 2017). In fact, it is a subject of ongoing research how well
 16 reanalyses fit the data they assimilate (Simmons et al., 2014, Wright and Hindley 2018). The
 17 data assimilation systems combine information from a model, a set of observations and a priori
 18 information weighted by their respective uncertainties. The degraded vertical resolution of the
 19 reanalyses, compared to radiosonde and GNSS-RO data also leads to differences, especially for
 20 derived quantities such as the tropopause location and temperature, which will be investigated
 21 in the following evaluations.

22 The reanalysis models resolve the TTL with different vertical resolutions, as illustrated in **Fig.**
 23 **1**. The number of model levels between 200 and 70 hPa varies among the reanalyses from a
 24 low of 4 (NCEP-NCAR R1) to a high of 21 (ERA5), corresponding to vertical resolutions
 25 between ~ 1.5 km and ~ 0.2 km. In addition to the native model levels, all reanalyses provide
 26 post-processed data on standard pressure levels with at least four levels situated between 200
 27 and 70 hPa (**Fig. 1**). The horizontal resolutions of the reanalysis products are approximately
 28 $0.25^\circ \times 0.25^\circ$ (ERA5), $0.7^\circ \times 0.7^\circ$ (ERA-Interim), $0.63^\circ \times 0.5^\circ$ (MERRA-2), $0.66^\circ \times 0.5^\circ$
 29 (MERRA), $0.56^\circ \times 0.56^\circ$ (JRA-55), $1.13^\circ \times 1.13^\circ$ (JRA-25), $0.5^\circ \times 0.5^\circ$ (CFSR), and $1.9^\circ \times 1.9^\circ$
 30 (R1).
 31

1



2

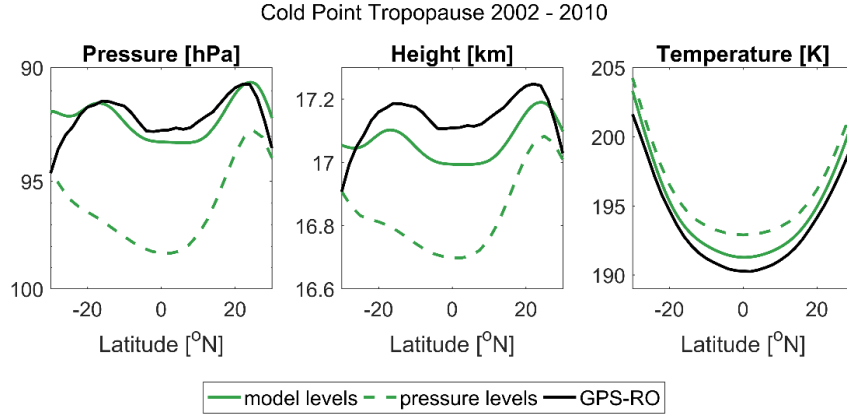
3 **Figure 1.** Model-level pressure values for different reanalysis data sets in the TTL using a fixed surface
4 pressure of 1013.25 hPa. Standard pressure levels (PL) in the TTL region are also shown.

5

6 **2.3 Methods**

7 Given the strong gradients of temperature and static stability in the TTL, the vertical resolution
8 of the reanalysis data sets is an important factor in cold point and lapse rate tropopause
9 calculations. For each reanalysis, tropopause heights and temperatures can be derived either
10 from model- or pressure-level data (**Fig 1**). A comparison of the CFSR cold point tropopause
11 based on model- and pressure-level temperature data is shown here to demonstrate the clear
12 advantage of the finer model-level resolution (**Fig. 2**). The cold point tropopause from CFSR
13 model-level data for the time period 2002–2010 agrees well with radio occultation results, with
14 differences of less than 1.5 K and 0.2 km at all latitudes. The tropopause derived from CFSR
15 pressure-level data, on the other hand, shows larger differences. This estimate is up to 0.4 km
16 too low and up to 3 K too warm, illustrating the need to use data with high vertical resolution
17 to identify and describe the tropopause. We derive the cold point and lapse rate tropopause
18 characteristics for each reanalysis using model-level data between 500 and 10 hPa at each grid
19 point at 6-hourly temporal resolution. Zonal and long-term averages are calculated by averaging
20 over all grid points, and represent the final step of data processing. For our calculations, the
21 cold point tropopause is defined as the coldest model level. The lapse rate tropopause is defined
22 as the lowest level at which the lapse rate decreases to 2 K km^{-1} or less, provided that the
23 average lapse rate between this level and all higher levels within 2 km does not exceed 2 K km^{-1}
24 ¹ (World Meteorological Organization, 1957).

25



1

2 **Figure 2.** Latitudinal distributions of zonal-mean cold point tropopause pressure (left), altitude (centre)
 3 and temperature (right) based on radio occultation data (black) and CFSR model-level (green solid) and
 4 pressure-level (green dashed) data during 2002–2010.

5

6 The evaluation of the interannual variability (Section 4) is based on time series of
 7 deseasonalized monthly temperature, pressure and altitude anomalies calculated relative to the
 8 mean annual cycle during 2002–2010. To study variability driven by tropospheric and
 9 stratospheric forcing, we identify and isolate the variations based on a standard multivariate
 10 regression analysis:

$$11 \quad T(t) = A_1 \cdot \text{QBO1}(t) + A_2 \cdot \text{QBO2}(t) + B \cdot \text{ENSO}(t) + D \cdot \text{VOL}(t). \quad (1)$$

12 Here $\text{QBO1}(t)$ and $\text{QBO2}(t)$ are orthogonal time series representing QBO variations constructed
 13 as the first two EOFs of the Freie Universität Berlin (FUB) radiosonde stratospheric winds
 14 (Naujokat, 1986). $\text{ENSO}(t)$ is the multivariate ENSO index
 15 (<https://www.esrl.noaa.gov/psd/enso/mei/>) and $\text{VOL}(t)$ is the stratospheric aerosol optical depth
 16 from the Global Space-based Stratospheric Aerosol Climatology (Thomason et al., 2018). The
 17 standard error of the regression coefficients was derived based on the bootstrap method (Efron
 18 and Tibshirani, 1993). The QBO temperature amplitude is calculated as the difference between
 19 the averaged maxima and averaged minima values of the time series of the QBO temperature
 20 variations $A_1 \cdot \text{QBO1}(t) + A_2 \cdot \text{QBO2}(t)$. For each QBO cycle of this time series, the absolute
 21 temperature maximum and minimum are selected. In a second step, the means over all such
 22 temperature maxima and minima are calculated to give the averaged maximum and minimum
 23 values, respectively.

24

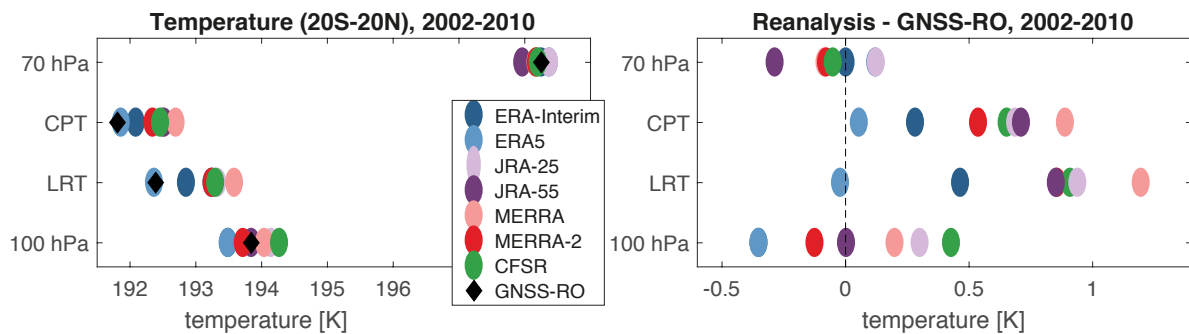
25 The long-term trends of the reanalyses temperature time series have been derived as the
 26 regression coefficient of a linear function that provides the best fit in a least-squares sense. The
 27 uncertainty in each long-term trend is calculated as the standard error of the slope with the
 28 effective sample size adjusted to account for the corresponding lag-1 autocorrelation
 29 coefficient. Significance is tested based on two-tailed test with a 95% confidence interval.

3 Temperature and tropopause characteristics

2

3 Tropical mean temperatures from reanalyses at two standard pressure levels (100 hPa and 70 hPa)
 4 hPa) and at the two tropopause levels are compared to radio occultation data for the time period
 5 2002–2010 (**Fig. 3**). At 100 hPa, reanalysis temperatures agree well with radio occultation data
 6 with differences between -0.35 K (too cold; ERA-Interim and ERA5) and 0.43 K (too warm;
 7 CFSR). At 70 hPa, the agreement is even better, with differences ranging from -0.29 K (JRA-
 8 55) to 0.12 K (JRA-25). However, nearly all reanalyses show warm biases at both tropopause
 9 levels, with differences of up to 1.2 K compared to the observations. Most likely, the excess
 10 warmth of tropopause estimates based on reanalysis products stems from the limited vertical
 11 resolution of the reanalysis models in the TTL region. The best agreement is found for the
 12 reanalysis with the highest vertical resolution (ERA5; 0.05 K too warm at the cold point
 13 tropopause). The data set with the lowest vertical resolution (NCEP-NCAR R1) is 2.2 K too
 14 warm, outside the range displayed in Figure 3.

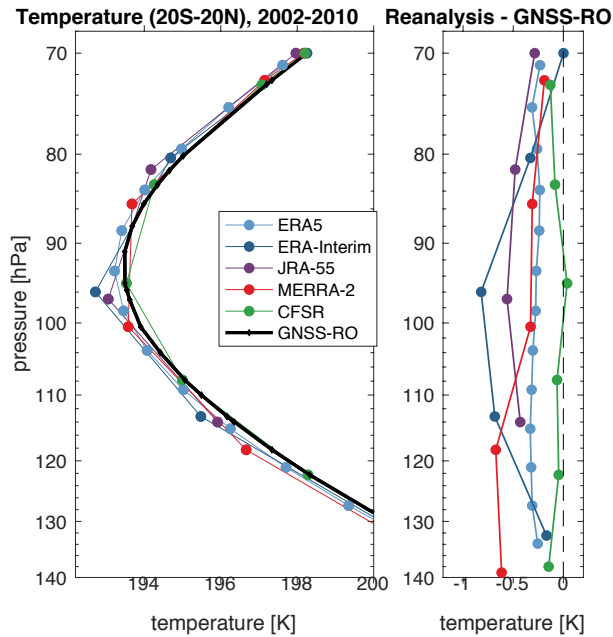
15



16

17 **Figure 3.** Tropical mean (20°S - 20°N) temperatures at 100 hPa, the lapse rate tropopause (LRT), the
 18 cold point tropopause (CPT) and 70 hPa from reanalyses and GNSS-RO data during 2002–2010 (left
 19 panel). Differences between the GNSS-RO and reanalysis temperatures are shown in the right panel. At
 20 100 hPa, ERA-Interim is hidden by ERA-5, at the LRT, MERRA-2 is hidden by JRA-55, and at 70 hPa,
 21 ERA5 is hidden by JRA-25 and MERRA is hidden by MERRA-2.

22 Temperature profile comparisons between 140 and 70 hPa at the native model levels ~~resolution~~
 23 have been conducted for the five most recent reanalyses (ERA5, ERA-Interim, JRA-55,
 24 MERRA-2, CFSR). All reanalyses tend to be colder than the observations in the tropical mean
 25 (**Fig. 4**), but differences are relatively small and the agreement is good overall. CFSR and ERA5
 26 agree best with the radio occultation data with mean biases of around -0.06 K and -0.28 K,
 27 respectively, averaged over the whole vertical range. ERA-Interim and MERRA-2 agree very
 28 well at upper levels but show large deviations on model levels near 100 hPa (ERA-Interim; $-$
 29 0.82 K) and below 110 hPa (MERRA-2; -0.67 K), respectively. The evaluation demonstrates
 30 that temperature comparisons at standard pressure levels (**Fig. 3**) can be biased by up to 0.5 K,
 31 with CFSR showing a positive bias (0.45 K) at the 100 hPa standard pressure level but very
 32 good agreement (-0.05 K) at nearby native model levels. Such biases can result from vertical
 33 interpolation of temperature data in regions with large lapse rate changes.



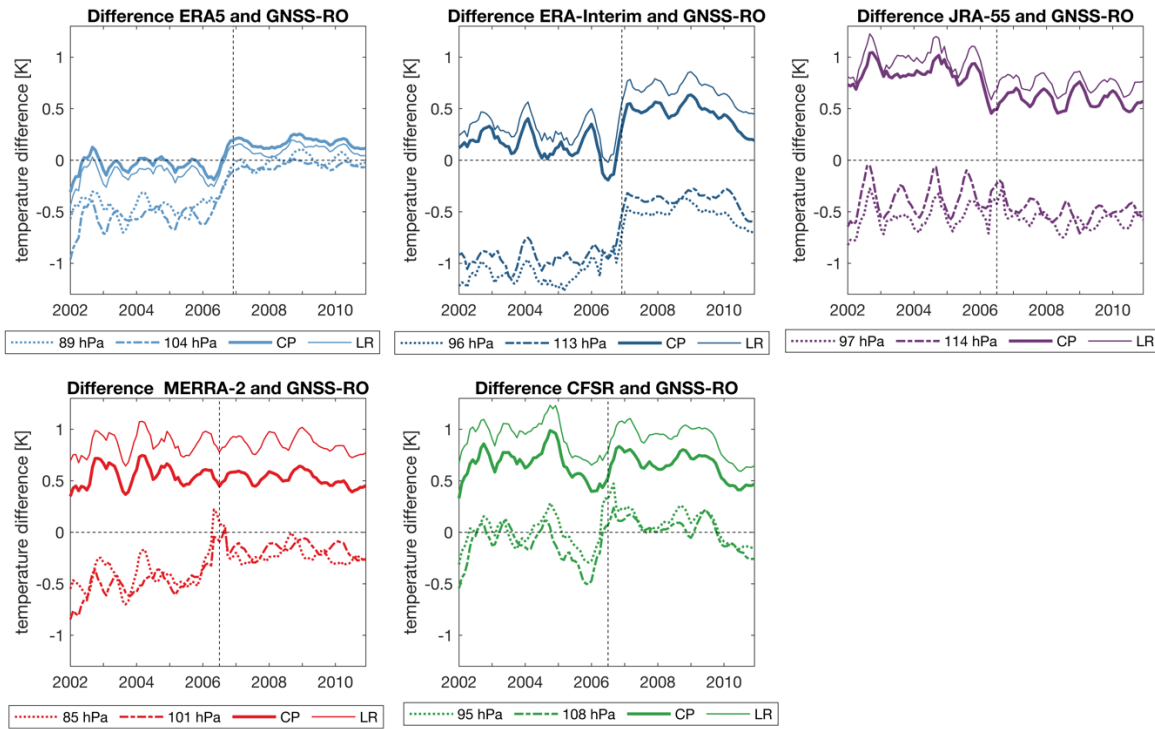
1
2 **Figure 4.** Tropical mean (20°S–20°N) temperature profiles at reanalysis model levels between 140 and
3 70 hPa (left panel) during 2002–2010 and differences between reanalysis and GNSS-RO temperatures
4 (right panel).

5
6 Comparing the temperature profiles to the tropopause values (**Fig. 3 and 4**) reveals that despite
7 the five reanalyses having negative biases at model levels, they mostly have positive biases at
8 the cold point and lapse rate tropopause levels. As the discrete values corresponding to
9 reanalysis model levels are unable to reproduce the true minimum temperature as recorded in a
10 near-continuous profile, this difference is expected for the cold point tropopause. Similarly, the
11 lapse rate tropopause criteria might typically be fulfilled at lower levels for data at coarser
12 resolution, thus resulting in a warm bias at the lapse rate tropopause on average. Overall, our
13 results indicate that the negative temperature bias at model levels is more than cancelled out by
14 the positive bias introduced when calculating the cold point and lapse rate tropopauses. Linking
15 the temperature profile and tropopause comparisons, this ‘bias shift’ is about 0.3 K for ERA5,
16 0.6 K for CFSR and 1 K or larger for ERA-Interim, MERRA-2 and JRA-55. In consequence,
17 ERA5, with both a small negative bias at the model levels and a small bias shift provides the
18 most realistic tropopause temperatures. CFSR also has a relatively small bias shift, but the
19 relatively unbiased temperature profile does not permit any error cancelation via this shift, so
20 that cold point and lapse rate tropopause levels based on CFSR are systematically too warm.

21 Agreement between the reanalysis temperature profiles and GNSS-RO data clearly improves
22 when the comparison is restricted to the 2007–2010 time period, when the more densely-
23 sampled COSMIC data were assimilated (**Table 1**). This point is illustrated by comparison of
24 temperature time series from reanalyses and observations at two model and both tropopause
25 levels (**Fig. 5**). For ERA5, ERA-Interim and MERRA-2, the cold bias with respect to GNSS-
26 RO at model levels decreases after 2007, most likely because of the high number of daily
27 COSMIC profiles available for assimilation from this time onwards. Cold biases at model levels
28 are accompanied by warm biases in the tropopause temperatures, which, for ERA-Interim and
29 ERA5, increase after 2007. As the increase at all levels is very similar, this indicates that the

1 advantage of a reduced temperature bias at model levels comes at the expense of an increased
 2 temperature bias at the tropopause. CFSR and MERRA-2 show no such systematic change of
 3 their tropopause temperatures over time when compared to GNSS-RO data. JRA-55 is the only
 4 reanalysis product for which cold point and lapse rate tropopause temperatures agree slightly
 5 better with GNSS-RO estimates after 2007.

6



7

8 **Figure 5.** Tropical mean (20°S - 20°N) time series of temperature differences between reanalysis and
 9 radio occultation at the cold point (CP) and lapse rate (LR) tropopause levels, as well as selected
 10 reanalysis model levels. Vertical lines indicate when the assimilation of COSMIC radio occultation data
 11 started.

12

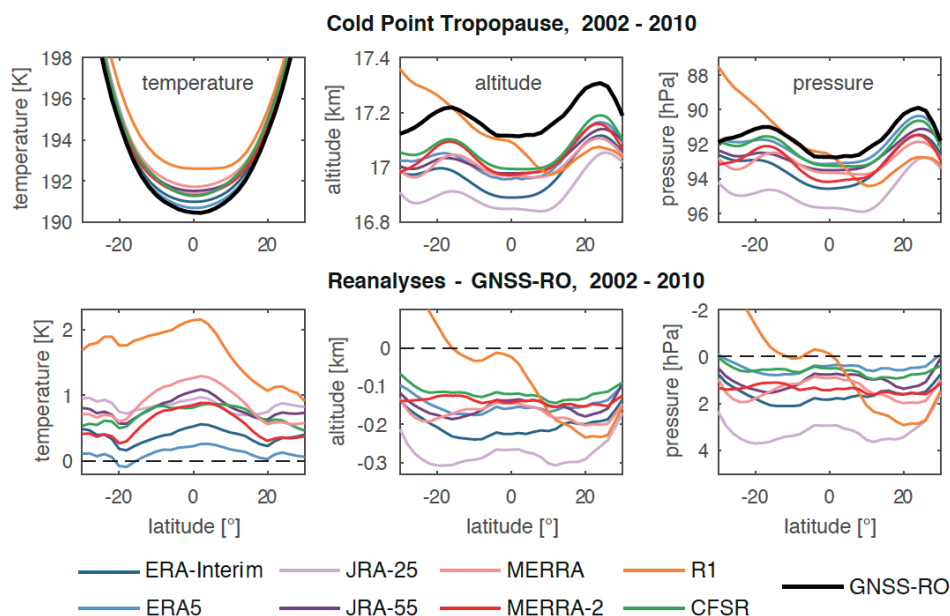
13 Evaluations of the latitudinal structure of the cold point tropopause for 2002–2010 are based on
 14 comparisons to radio occultation data (**Fig. 6**). All reanalysis data sets produce tropopause
 15 levels that are too low and too warm, with the latter related to vertical resolution as explained
 16 above. The observations show that average cold point temperatures are lowest right around the
 17 equator. The reanalyses fail to reproduce this latitudinal gradient, indicating more constant cold
 18 point temperatures across the inner tropics between 10°S and 10°N with a less pronounced
 19 minimum at the equator. As a consequence, the largest differences in cold point tropopause
 20 temperatures relative to GNSS-RO data are at the equator and the best agreement is around
 21 $20^{\circ}\text{S}/20^{\circ}\text{N}$ for all reanalysis data sets.

22

23

1 The cold point altitude and pressure exhibit little north–south variability, ranging from 16.9 km
 2 (94 hPa) to 17.2 km (91.8 hPa). With respect to the seasonal cycle, it is well known that the
 3 temperature and altitude of the cold point tropopause are linked, with the coldest temperatures
 4 and highest altitudes observed during boreal winter (e.g., Seidel et al., 2001; Kim and Son,
 5 2012). This relationship does not hold in the meridional direction: the highest cold point
 6 altitudes are located around 20°S/20°N, while the lowest cold point temperatures are located
 7 near the equator. The higher altitude/lower pressure of the cold point tropopause around
 8 20°S/20°N results from zonally-variable features linked to tropospheric pressure regimes, such
 9 as particularly low tropopause pressures over the Tibetan plateau during boreal summer (Kim
 10 and Son, 2012). The reanalysis data sets capture most of this latitudinal structure, showing
 11 roughly constant differences between about 0.1 and 0.2 km (0–2 hPa). The largest differences
 12 are found for NCEP-NCAR R1 in the Southern Hemisphere, where the cold point tropopause
 13 based on R1 is both higher and warmer than observed. The best agreement with respect to cold
 14 point temperatures is found for ERA5 and ERA-Interim, which are around 0.2 K and 0.4 K
 15 warmer than the radio occultation data, respectively. All other reanalysis data sets are in close
 16 agreement with each other, with differences from the observations of between 0.5 K and 1 K.
 17 The altitude and pressure of the cold point tropopause are captured best by ERA5, CFSR,
 18 MERRA, MERRA-2 and JRA-55, which all produce cold point tropopauses that are slightly
 19 too low (~0.1 km). ERA-Interim, despite very good agreement in cold point temperature, shows
 20 slightly larger biases in cold point altitude (~0.2 km) relative to the GNSS-RO benchmark.
 21 Zonal mean cold point tropopause temperatures, altitudes and pressures during 1981-1990 and
 22 1991-2002 are shown for all reanalyses in the supplementary Figure S1.

23

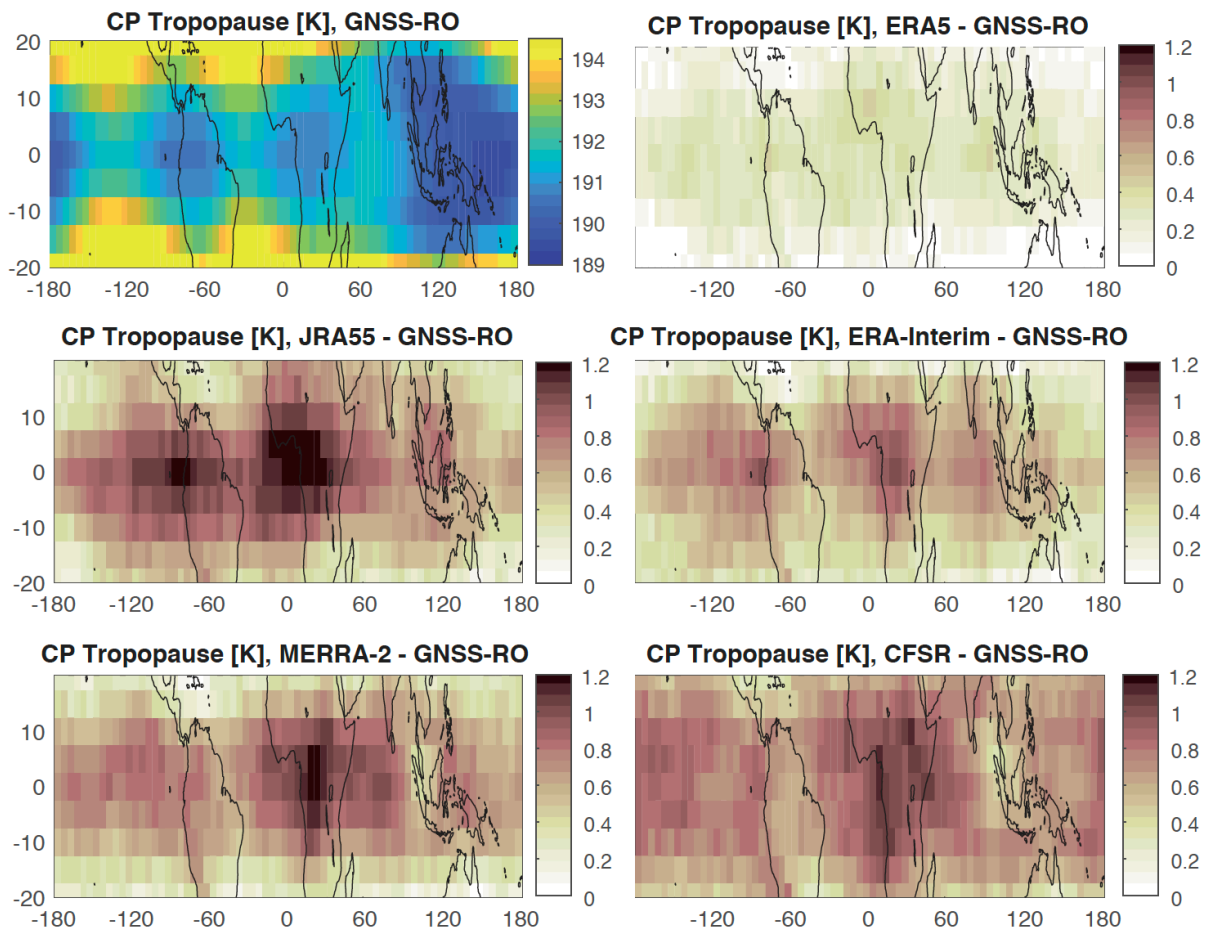


24

25 **Figure 6.** Latitudinal distributions of zonal-mean cold point tropopause temperature (left), altitude
 26 (centre) and pressure (right) based on radio occultation data and reanalysis products during 2002–2010
 27 (upper row). Differences between radio occultation and reanalysis estimates are shown in the lower row.

1 We investigate the temperature biases and their maxima near the equator by analysing latitude–
 2 longitude variations in the cold point tropopause relative to GNSS-RO estimates for four of the
 3 reanalyses (**Fig. 7**). To show differences at relatively high spatial resolution, we focus on the
 4 period 2007–2010. A wealth of observational studies has shown that the coldest tropopause
 5 temperatures are located over the “maritime continent” (i.e. the general area of Indonesia) and
 6 the West Pacific (Highwood and Hoskins, 1998), with secondary minima over equatorial South
 7 America and Africa coinciding with other centres of deep convective activity (Gettelman et al.,
 8 2002). The collocation of tropospheric convective activity with zonal asymmetries in cold point
 9 temperature can be explained by the radiative cooling effects of cirrus clouds overlying deep
 10 convection (Hartmann et al., 2001) or diabatic cooling associated with convective detrainment
 11 (Sherwood et al., 2003). Furthermore, it has been suggested that the response of equatorial
 12 waves to convective heating influences the structure of the cold point tropopause (Kim and Son,
 13 2012; Nishimoto and Shiotani, 2012; Nishimoto and Shiotani, 2013). The dominant wave
 14 modes responsible for cold point temperature variability are linked to equatorial Kelvin waves
 15 and the Madden-Julian oscillation.

16



17

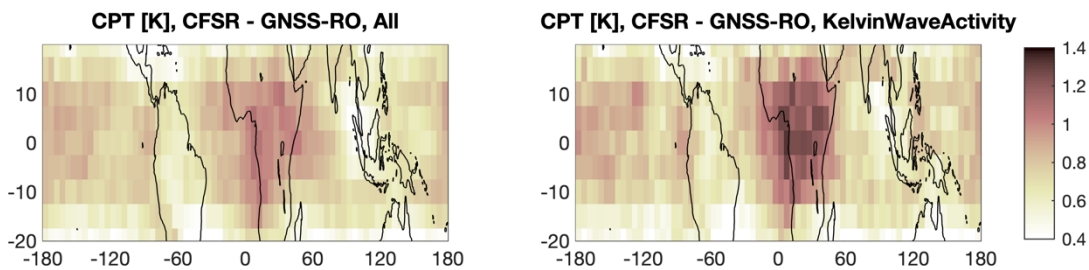
18 **Figure 7.** Latitude–longitude distributions of annual mean GNSS-RO cold point temperatures (upper
 19 left) and differences between cold point temperatures from individual reanalyses and those from GNSS-
 20 RO during 2007–2010 (lower panels).

21

1 For the analysed reanalyses (ERA5, ERA-Interim, MERRA-2, JRA55, and CFSR), differences
2 with respect to the observations are largest in the inner tropics over central Africa, reaching
3 values 50% to 100% greater than the zonal mean differences. This region is characterized by a
4 local cold point minimum that results from deep convection and its interaction with equatorial
5 waves. There is also evidence of a secondary maximum in the differences over equatorial South
6 America or the East Pacific, although the magnitude and location of this maximum differ among
7 the reanalyses.

8 The convective centre over the Western Pacific warm pool, where the cold point tropopause is
9 coldest, does not show enhanced biases relative to the observations. One possible explanation
10 for the bias distribution might link the enhanced temperature differences to Kelvin wave activity
11 that maximizes over Central Africa but is weaker over the West Pacific (Kim et al., 2019). As
12 the Kelvin waves disturb the temperature profile at small vertical scales, the reanalyses may be
13 particularly unsuited to estimate cold point temperatures in regions of strong Kelvin wave
14 activity. We average cold point temperatures from reanalyses and observations over time
15 periods of enhanced Kelvin wave activity. For CFSR, composite differences for periods with
16 enhanced wave activity are compared in **Fig. 8** to mean differences averaged over the whole
17 2007–2010 period. While mean biases over Central Africa are less than 1 K, average differences
18 during periods of enhanced Kelvin wave activity are as large as 1.4 K. The same is true for
19 other reanalyses (not shown here), with the exception of ERA-Interim, suggesting that in most
20 cases Kelvin waves contribute to the spatial structure of biases in cold point tropopause
21 estimates based on reanalysis products.

22



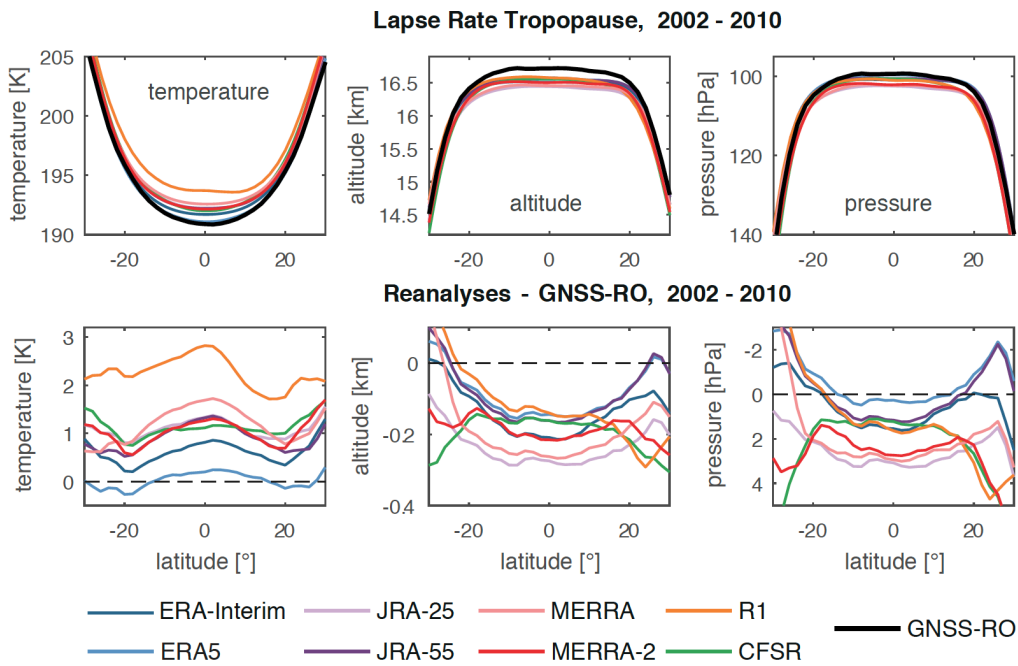
24 **Figure 8.** Latitudinal-longitude sections of the differences between GNSS-RO and CFSR cold point
25 temperatures for 2007-2010 (left panel) and for time periods of high wave activity (right panel).

26

27 The zonal mean lapse rate tropopause (**Fig. 9**) at the equator is found at similar temperatures
28 and heights as the cold point tropopause, being only slightly warmer and lower. Poleward of
29 10°S/10°N, however, the lapse rate tropopause height decreases considerably faster than the
30 cold point height, since the cold point is more often located at the top of the inversion layer
31 while the lapse rate tropopause is located at the bottom of the inversion layer (Seidel et al.,
32 2001). Lapse rate tropopause temperatures based on reanalysis data are on average about 0.2 K
33 to 1.5 K too warm when compared to radio occultation data (see **Fig. 3** and associated
34 discussion) with best agreement for ERA5 and ERA-Interim. Consistent with this temperature
35 bias, lapse rate tropopause levels based on reanalysis data are about 0.2 km to 0.4 km lower

1 than those based on radio occultation data. The latitudinal structure of lapse rate tropopause
 2 temperatures reveals slightly larger biases at the equator and better agreement between 10°–20°
 3 in each hemisphere, and is generally very similar to the latitudinal distribution of biases in cold
 4 point temperatures (**Fig. 6**). The altitude of the lapse rate tropopause shows considerable zonal
 5 meridional variability, ranging from 14.5 km to 16.7 km. All reanalyses capture the plateau in
 6 lapse rate tropopause altitudes between 20°S and 20°N and the steep gradients in these altitudes
 7 on the poleward edges of the tropics. Zonal mean lapse rate tropopause temperatures, altitudes
 8 and pressures during 1981-1990 and 1991-2002 are shown for all reanalyses in the
 9 supplementary Figure S2.

10



11

12 **Figure 9.** Latitudinal distributions of zonal-mean lapse rate tropopause temperature (left), altitude
 13 (centre) and pressure (right) based on radio occultation data and reanalysis products during 2002–2010
 14 (upper row). Differences between radio occultation and reanalysis estimates are shown in the lower row.

15

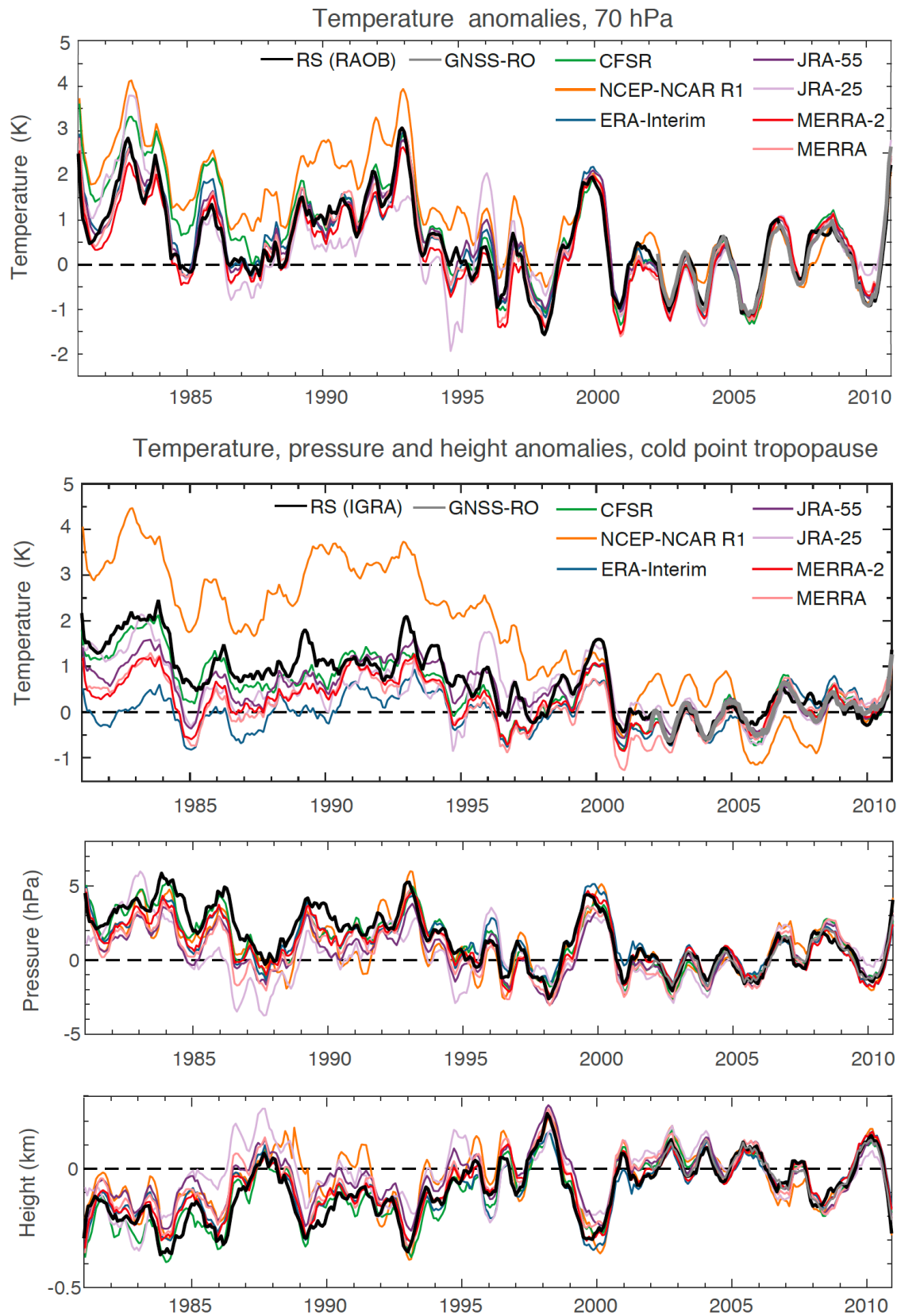
16

17

4 Interannual variability and long-term changes

It has long been recognized that inter-annual variations in TTL temperatures are strongly affected by both tropospheric (e.g. ENSO) and stratospheric (e.g. QBO, solar, volcanic) variability (Randel et al., 2000; Zhou et al., 2001, Krüger et al 2008). Time series of deseasonalized monthly 70 hPa temperature anomalies and cold point temperature, pressure and altitude anomalies are shown in **Fig. 10**. Anomalies are calculated relative to the mean annual cycle during 2002–2010 for each dataset. The interannual variability of ERA5 is not analysed due to the short data record available at the time of the analysis. The performance of the reanalyses with respect to both the spread among reanalyses and their agreement with observations is much better at the 70 hPa level than at the cold point level. The older reanalyses NCEP-NCAR R1 and JRA-25 generally show larger deviations from the RAOBCORE time series. The level of agreement among the reanalyses and between reanalyses and observations improves over time, with a step-like improvement around 1998–1999 that is likely associated with the TOVS-to-ATOVS transition. The higher vertical resolution of measurements from the ATOVS suite (see, e.g. Figure 7 in Fujiwara et al., 2017) is known to reduce differences among the reanalysis with respect to stratospheric temperature (Long et al., 2017) and polar diagnostics (Lawrence et al., 2018). Within the TTL, temperature biases decrease from values of 1–2 K to around 0.5 K following the TOVS-to-ATOVS transition. This agreement improves further after 2002, when many of the more recent reanalyses started assimilating AIRS and GNSS-RO data (**Table 1**; see also Figure 8 in Fujiwara et al., 2017).

Interannual variability at 70 hPa is dominated by the stratospheric QBO signal, which is reproduced by all reanalysis data sets. The amplitudes of the QBO temperature variations in all datasets based on a multilinear regression analyses over 1981–2010 are shown in **Fig. 11**. At 70 hPa, the observational radiosonde data sets give QBO variations of 2.1–2.2 K. Reanalyses agree well with the observations and show QBO variations of 2–2.4 K. The only exception is NCEP-NCAR R1, which clearly underestimates the signal compared to radiosondes and other reanalyses, with an amplitude of 1.7 K. Best agreement with the radiosonde data sets is found for MERRA-2, MERRA and CFSR. The influence of ENSO on TTL temperatures (not shown here) shows large longitudinal variations with positive anomalies over the maritime continent and West Pacific and negative anomalies over the East Pacific. While the zonally resolved response patterns agree well between observations and reanalyses, the zonal mean responses are not significant. Positive temperature anomalies following the eruptions of El Chichón in 1982 can be detected in Fig. 10 for all reanalyses, consistent with the results of Fujiwara et al. (2015). Following the Mount Pinatubo eruption in 1991, small positive temperature anomalies are evident at the 70 hPa level around the beginning of 1992. However, no positive temperature anomalies are found at the cold point during this time (see Fujiwara et al., 2015 for a more detailed analysis).



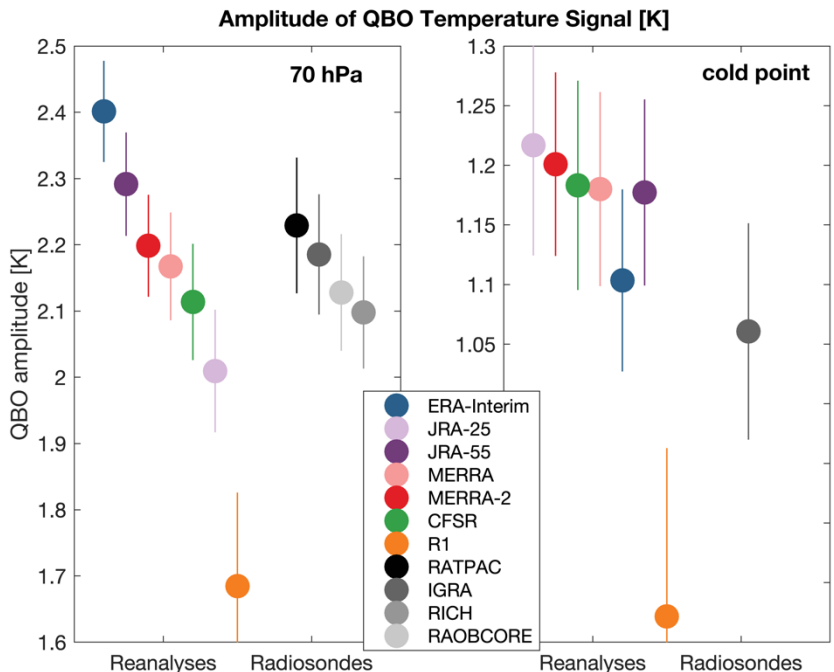
1

2 **Figure 10.** Time series of deseasonalized anomalies in 70 hPa temperature (upper), cold point
 3 temperature (upper middle), cold point pressure (lower middle) and cold point altitude (lower) averaged
 4 over the tropics (20°S–20°N) and evaluated relative to the reference period 2002–2010. Time series are
 5 shown for reanalysis products, radiosonde data (RAOBCORE and IGRA) and radio occultation data
 6 (GNSS-RO). Time series are smoothed with a 7-months running mean.

1 At the cold point, NCEP-NCAR R1 is a clear outlier, with much warmer temperature anomalies
 2 than any other data set during the period prior to 2005 (Fig. 10). However, differences among
 3 the more recent reanalyses are also relatively large, with ERA-Interim (on the lower side) and
 4 CFSR (on the upper side) showing differences as large as 2 K in the early years of the
 5 comparison. Given that existing homogenized radiosonde data sets also show deviations of up
 6 to 1.5 K at this level (Figure 2 in Wang et al., 2012), we cannot deduce which reanalysis data
 7 set is most realistic. Note that the radiosonde time series from IGRA shown here should not be
 8 used for evaluating long-term changes (see Wang et al., 2012 for details), but only for assessing
 9 the representation of interannual variability. Periods of particularly pronounced interannual
 10 variability alternate with relatively quiescent ones. The amplitude of interannual variability
 11 (Fig. 10) and the QBO temperature signal (Fig. 11) are weaker at the cold point than at 70 hPa,
 12 but are still well captured by all of the reanalysis data sets except for NCEP-NCAR R1.

13
 14 Interannual variability in cold point pressure and altitude (Fig. 10) shows better agreement
 15 among the data sets than that in cold point or 70 hPa temperature. During the first 15 years of
 16 the record, the reanalysis cold point tropopause levels are mostly shifted toward higher
 17 altitudes and higher pressures, consistent with higher temperatures during this period.
 18 Anomalies in cold point temperature are in most cases matched by anomalies in cold point
 19 pressure and altitude, with a warmer cold-point temperature (e.g. around 1999–2000)
 20 corresponding to lower tropopause (negative altitude anomaly and positive pressure anomaly)
 21 and vice versa. The older reanalyses NCEP-NCAR R1 and JRA-25 again show the largest
 22 overall differences. The agreement improves over time, with the most consistent results found
 23 for the period after 2002.

24
 25

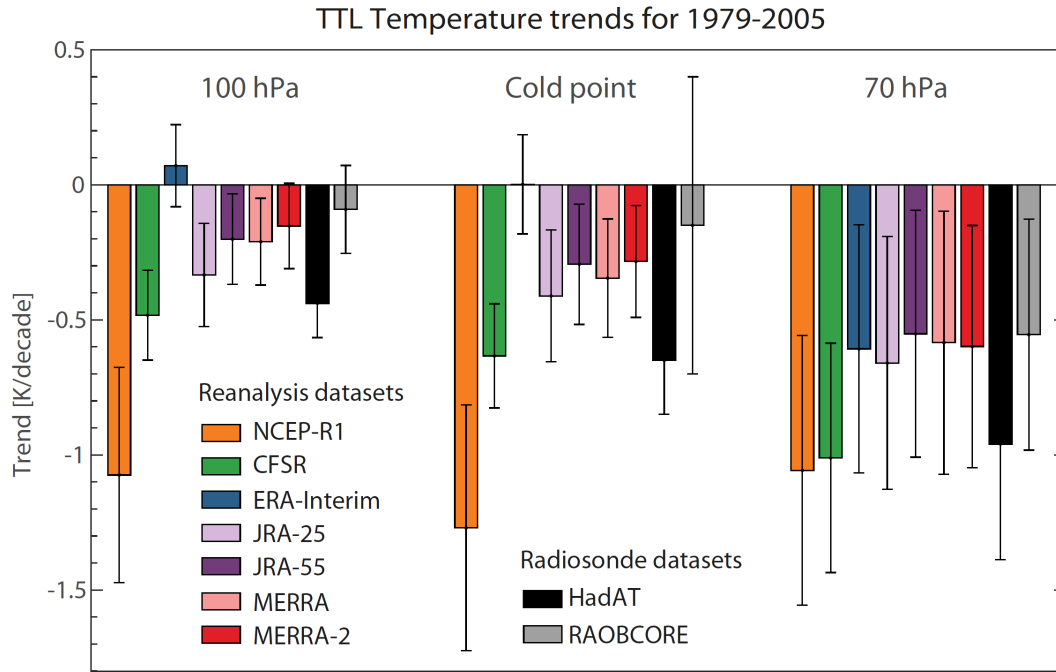


26
 27 **Figure 11.** Amplitude of QBO temperature signal for 10°S-10°N at 70 hPa and the cold point derived
 28 from a multilinear regression analyses for radiosonde and reanalysis data sets for the period 1981-2010.

1 Long-term temperature changes are evaluated over the 1979-2005 time period due to the
2 availability of adjusted tropopause trends from radiosonde data sets (see Wang et al., 2012 for
3 details). Both radiosonde records suggest significant cooling at the 70 hPa level (**Fig. 12**).
4 Trends derived from reanalysis data can be problematic due to changes in the assimilated
5 observations. Given this potential limitation, it is of interest to examine whether the reanalysis
6 trends are consistent with the hypothetically more reliable trends derived from homogenized
7 observational records. At 70 hPa, temperature trends based on the reanalysis data sets span
8 almost exactly the same range (-0.5 to -1.1 K/decade) as those based on the radiosonde data
9 sets (-0.5 to -1 K/decade). All reanalysis- and observationally-based trends are significant at
10 this level, confirming the stratospheric cooling reported by many previous studies (e.g., Randel
11 et al., 2009). Satellite data from the Microwave Sounding Unit channel 4 (~ 13 – 22 km) suggests
12 smaller trends of around -0.25 K/decade over 1979–2005 (Maycock et al., 2018) or -0.4
13 K/decade over 1979–2009 (Emanuel et al., 2013). However, the much broader altitude range
14 of this MSU channel includes both stratospheric and tropospheric levels, which impedes a direct
15 comparison with trends at 70 hPa.

16 At the 100 hPa and cold point levels, the situation is completely different. The available
17 adjusted radiosonde data sets show in some cases uncertainties larger than the respective
18 temperature trends at these levels. Only a few of the available data sets indicate a statistically
19 significant cooling based on a methodology that adjusts the cold point trend to account for
20 nearby fixed pressure-level data and day–night differences (Wang et al., 2012). Based on the
21 trends shown in Wang et al. (2012) for five adjusted radiosonde data sets, we show here the
22 smallest and largest reported trends and consider their range (including the reported error bars)
23 as the observational uncertainty range. Similar to the observations, the reanalysis data sets
24 suggest a large range in cold point temperature trends, from no trend at all (0 K/decade for
25 ERA-Interim) to a strong cooling of -1.3 K/decade (NCEP-NCAR R1). The latter is outside of
26 the observational uncertainty range and can thus be considered unrealistic. All other reanalyses
27 suggest small but significant cooling trends of -0.3 K/decade to -0.6 K/decade. JRA-25, JRA-
28 55, MERRA, and MERRA-2 agree particularly well and produce trends in the middle of the
29 observational uncertainty range. Overall, due to the large uncertainties in radiosonde-derived
30 cold point temperature trends, all reanalyses except for R1 are statistically consistent with at
31 least one of the observational data sets.

32



1

2 **Figure 12.** Linear trends in tropical mean (20°S – 20°N) temperature (K/decade) at 100 hPa, the
 3 cold point and 70 hPa for the time period 1979–2005. Error bars indicate $\pm 2\sigma$ uncertainty in the trend and
 4 account for serial auto-correlation.

5 Temperature trends at 100 hPa are very similar to trends at the cold point level, and again
 6 suggest consistency among most of the reanalysis and radiosonde data sets, with the notable
 7 exception of R1. Nearly all data sets suggest slightly smaller cooling trends (-0.15 K/decade to
 8 -0.5 K/decade) relative to the cold point consistent with the fact that the cold point is at slightly
 9 higher altitudes than 100 hPa. Among the data sets, only ERA-Interim produces a warming
 10 trend (0.07 K/decade), although this result is not statistically significant.

11

12 **5 Summary**

13 Meteorological reanalyses are widely used in scientific studies of TTL processes being utilized
 14 as “stand in observations” or for driving transport models. The most recent atmospheric
 15 reanalysis data sets (ERA5, ERA-Interim, MERRA-2, JRA-55, and CFSR) all provide realistic
 16 representations of the major characteristics of temperature structure within the TTL for 2002–
 17 2010. There is good agreement between reanalysis estimates of tropical mean temperatures
 18 between 140 and 70 hPa and GNSS-RO retrievals, with relatively small cold biases for most
 19 data sets. CFSR shows the best agreement with GNSS-RO in this layer with a mean bias of $-$
 20 0.06 K. Agreement between the temperature profiles and the GNSS-RO data clearly improves
 21 when the comparison is restricted to the period after 2007, when the densely-sampled COSMIC
 22 data were assimilated by all reanalyses.

23 Temperatures at the cold point and lapse rate tropopause levels show warm biases in reanalyses
 24 when compared to observations. This tropopause-level warm bias is opposite to the cold bias
 25 found at all model levels and is most likely related to difficulties in determining the true cold

1 point and lapse rate tropopause levels from discrete temperature profiles with coarse vertical
2 resolution. Our analysis confirms that the magnitude of the bias shift is consistent with the
3 vertical resolution of the reanalysis data, with the smallest bias shifts found for data sets with
4 the highest vertical resolution around the tropopause (ERA5 and CFSR). The negative
5 temperature bias at model levels is often cancelled out by the positive bias introduced when
6 identifying the lapse rate and cold point tropopause locations. As a result, ERA5, which has a
7 small negative bias at model levels and a small bias shift, has the most realistic tropopause
8 temperatures, while CFSR, which produces the most realistic model-level temperature profile,
9 has a warm bias of 0.6–0.9 K at the cold point and lapse rate tropopause levels. Older reanalyses
10 like MERRA, JRA-25 and especially NCEP-NCAR R1 show the largest temperature biases at
11 the tropopause levels.

12 The zonal structure of tropopause temperature reveals that the biases in reanalysis relative to
13 observations maximise at or near the equator. All of the recent reanalyses produce a realistic
14 horizontal structure of cold point temperature with minima corresponding to the centres of
15 tropical deep convection. Differences between reanalyses and observations are greatest over
16 equatorial Africa. These enhanced differences are possibly related to Kelvin wave activity and
17 associated disturbances in TTL temperatures that also maximize in this region. Further
18 investigation of seasonal variability in the cold point tropopause, including detailed analysis of
19 this feature, will be conducted in a follow-up study.

20 Interannual variability in reanalysis temperatures is best constrained in the upper TTL (70 hPa),
21 with larger differences at lower levels such as the cold point and 100 hPa. The reanalyses
22 reproduce the temperature responses to major dynamical and radiative signals such as volcanic
23 eruptions and the QBO. Agreement among the reanalyses and between the reanalyses and
24 observations generally improves over time, with a step-like improvement around the TOVS-to-
25 ATOVS transition in 1998–1999 and in 2006 with the beginning of assimilation of COSMIC
26 GNSS-RO data. Interannual variability is lower at the cold point and 100 hPa relative to 70
27 hPa, but with larger month-to-month fluctuations causing larger discrepancies among the
28 reanalyses. As at 70 hPa, NCEP-NCAR R1 is a clear outlier. Interannual variability in cold
29 point pressure and altitude shows better agreement than that in TTL temperature. Anomalies in
30 cold point temperatures are in most cases matched by corresponding anomalies in cold point
31 pressure and altitude.

32 Long-term reanalysis trends in temperature at 70 hPa show good agreement with trends derived
33 from adjusted radiosonde data sets. All reanalyses and observational data sets indicate
34 significant stratospheric cooling at this level of around -0.5 K/decade to -1 K/decade. At the
35 100 hPa and cold point levels, both adjusted radiosonde data sets and reanalyses indicate large
36 uncertainties in temperature trends. Reanalysis-based estimates at the cold point range from no
37 trend at all (0 K/decade for ERA-Interim) to strong cooling of -1.3 K/decade (NCEP-NCAR
38 R1). While the latter is outside of the observational uncertainty range and can be considered
39 unrealistic, all other reanalyses data sets agree with at least one of the observational data sets
40 within uncertainties. The bulk of the reanalyses are in good agreement at these levels,
41 suggesting small but significant cooling trends of -0.3 K/decade to -0.6 K/decade that are
42 statistically consistent with trends based on the adjusted radiosonde data sets.

1 Advances of the reanalysis and observational systems over the last decades have led to a clear
2 improvement of the TTL reanalyses products over time. In particular, the more recent
3 reanalyses ERA-Interim, ERA5, MERRA-2, CFSR and JRA-55 mostly show very good
4 agreement after 2002 in terms of the vertical TTL temperature profile, meridional tropopause
5 structure and interannual variability. Temperatures at the cold point and lapse rate, on the other
6 hand, are too high for most reanalyses, regardless of production date. As these differences
7 maximise over Central Africa, a centre of deep convective activity, chemistry-transport models
8 driven by reanalyses and simulating air mass transport into the stratosphere, can be expected to
9 have too little dehydrations and too high water vapor. Furthermore, all reanalyses place the cold
10 point tropopause too low in altitude relative to observations. This displacement can have
11 important implications for studies that compare water vapor and ice observations with the
12 position of the cold point tropopause derived from reanalyses data, as enhanced ice and water
13 vapour contents could be erroneously attributed to deep convection crossing the tropopause.

14 Depending on the particular application, different reanalyses offer different advantages such as
15 a realistic cold point temperature (e.g., ERA5), small bias in the TTL temperature profile (e.g.,
16 CFSR), realistic spatial distribution of the cold point temperature (e.g., ERA-Interim),
17 continuous TTL temperature time series through 2006 (e.g., JRA55), or a realistic
18 representation of signals of interannual variability (e.g., MERRA-2). Their use in model
19 simulations and in comparisons with climate model output should be tailored to their specific
20 strengths and weaknesses.

21 **Author contributions.** ST developed the idea for this paper and carried out the evaluations
22 with contributions from all co-authors. SD and BL provided the reanalyses tropopause and
23 profile data. RPK provided the GNSS-RO tropopause, wave activity and temperature profile
24 data. J. S. Wang provided the radiosonde tropopause data. ST wrote the manuscript with
25 contributions from all co-authors.

26 **Data availability.** Reanalyses, GNSS-RO and radiosonde data can be inquired about by
27 contacting the authors

28 **Competing interests.** The authors declare that they have no conflict of interest.

29 **Acknowledgements.** We thank the reanalysis centres for providing their support and data
30 products. We thank C. Bloecker from the Global Modeling and Assimilation Office, NASA
31 Goddard Space Flight Center for providing information on the GNSS-RO data assimilated in
32 MERRA-2. ERA5 data were generated using Copernicus Climate Change Service Information.
33 MERRA-2 data access was through the Global Modeling and Assimilation Office (GMAO,
34 2015). The work of S. Tegtmeier was funded by the Deutsche Forschungsgemeinschaft (DFG,
35 German Research Foundation) – TE 1134/1. Contributions from J.S. Wright were supported by
36 the National Natural Science Foundation of China (20171352419) via a joint DFG–NSFC
37 funding initiative.

1 **References**

- 2 Anthes, R. A., Bernhardt, P. A., Chen, Y., Cucurull, L., Dymond, K. F., Ector, D., Healy, S. B., Ho, S.-
3 P., Hunt, D. C., Kuo, Y.-H., Liu, H., Manning, K., McCormick, C., Meehan, T. K., Randel, W. J.,
4 Rocken, C., Schreiner, W. S., Sokolovskiy, S. V., Syndergaard, S., Thompson, D. C., Trenberth, K. E.,
5 Wee, T.-K., Yen, N. L., and Zeng, Z.: The COSMIC/FORMOSAT-3 Mission: Early Results, Bulletin
6 of the American Meteorological Society, 89, 313, <https://doi.org/10.1175/BAMS-89-3-313>, 2008.
- 7 Beyerle, G., Schmidt, T., Michalak, G., Heise, S., Wickert, J., and Reigber, C.: GPS radio occultation
8 with GRACE: Atmospheric profiling utilizing the zero difference technique, Geophysical Research
9 Letters, 32, L13806, <https://doi.org/10.1029/2005GL023109>, 2005.
- 10 Beyerle, G., Grunwaldt, L., Heise, S., Köhler, W., König, R., Michalak, G., Rothacher, M., Schmidt, T.,
11 Wickert, J., Tapley, B. D., and Giesinger, B.: First results from the GPS atmosphere sounding
12 experiment TOR aboard the TerraSAR-X satellite, Atmospheric Chemistry & Physics, 11, 6687–6699,
13 <https://doi.org/10.5194/acp-11-6687-2011>, 2011.
- 14 Chipperfield, M. P., Multiannual simulations with a three-dimensional chemical transport model, J.
15 Geophys. Res., 104(D1), 1781– 1805, doi:10.1029/98JD02597, 1999.
- 16 Cucurull, L., J. C. Derber, and R. J. Purser: A bending angle forward operator for global positioning
17 system radio occultation measurements. Journal of Geophysical Research: Atmospheres, 118, 14-28.
18 doi: 10.1029/2012JD017782, 2013.
- 19 Dee, D. P., Uppala, S. M., Simmons, A. J., Berrisford, P., Poli, P., Kobayashi, S., Andrae, U.,
20 Balmaseda, M. A., Balsamo, G., Bauer, P., Bechtold, P., Beljaars, A. C. M., van de Berg, L., Bidlot, J.,
21 Bormann, N., Delsol, C., Dragani, R., Fuentes, M., Geer, A. J., Haimberger, L., Healy, S. B., Hersbach,
22 H., Hólm, E. V., Isaksen, I., Kållberg, P., Köhler, M., Matricardi, M., McNally, A. P., Monge-Sanz, B.
23 M., Morcrette, J.-J., Park, B.-K., Peubey, C., de Rosnay, P., Tavolato, C., Thépaut, J.-N. and Vitart, F.:
24 The ERA-Interim reanalysis: configuration and performance of the data assimilation system. Q.J.R.
25 Meteorol. Soc., 137: 553–597. doi: 10.1002/qj.828, 2011.
- 26 Durre, I., R. S. Vose, and D. B. Wuertz, Overview of the Integrated Global Radiosonde Archive, J.
27 Clim., 19(1), 53–68, doi:10.1175/JCLI3594.1, 2006.
- 28 Efron, B., and R. J. Tibshirani, An Introduction to the Bootstrap, 436 pp., Chapman and Hall, New York,
29 1993.
- 30 Emanuel, K., S. Solomon, D. Folini, S. Davis, and C. Cagnazzo, Influence of Tropical Tropopause Layer
31 Cooling on Atlantic Hurricane Activity. J. Climate, 26, 2288–2301, <https://doi.org/10.1175/JCLI-D-12-00242.1>, 2013.
- 33 Folkins, I., M. Lowewenstein, J. Podolske, S. Oltmans, and M. Proffitt, A barrier to vertical mixing at
34 14 km in the tropics: Evidence from ozonesondes and aircraft measurements, J. Geophys. Res.,104,
35 22095-22102, 1999.
- 36 Free, M., Seidel, D. J., Angell, J. K., Lanzante, J., Durre, I., and Peterson, T. C., Radiosonde
37 Atmospheric Temperature Products for Assessing Climate (RATPAC): A new data set of large-area
38 anomaly time series, J. Geophys. Res., 110, D22101, doi:10.1029/2005JD006169, 2005
- 39 Fueglistaler S, Dessler A E, Dunkerton T J, et al., Tropical tropopause layer, Rev. Geophys., 47,
40 RG1004, doi:10.1029/2008RG000267, 2009.

- 1 Fueglistaler, S., Haynes, P. H., and Forster, P. M.: The annual cycle in lower stratospheric temperatures
2 revisited, *Atmos. Chem. Phys.*, 11, 3701-3711, <https://doi.org/10.5194/acp-11-3701-2011>, 2011.
- 3 Fujiwara, M., Suzuki, J., Gettelman, A., Hegglin, M. I., Akiyoshi, H., and Shibata, K., Wave activity in
4 the tropical tropopause layer in seven reanalysis and four chemistry climate model data sets, *J. Geophys.*
5 *Res.*, 117, D12105, doi:10.1029/2011JD016808, 2012.
- 6 Fujiwara, M., Hibino, T., Mehta, S. K., Gray, L., Mitchell, D., and Anstey, J.: Global temperature
7 response to the major volcanic eruptions in multiple reanalysis data sets, *Atmos. Chem. Phys.*, 15,
8 13507-13518, <https://doi.org/10.5194/acp-15-13507-2015>, 2015.
- 9 Fujiwara, M., Wright, J. S., Manney, G. L., Gray, L. J., Anstey, J., Birner, T., Davis, S., Gerber, E. P.,
10 Harvey, V. L., Hegglin, M. I., Homeyer, C. R., Knox, J. A., Krüger, K., Lambert, A., Long, C. S.,
11 Martineau, P., Molod, A., Monge-Sanz, B. M., Santee, M. L., Tegtmeier, S., Chabrillat, S., Tan, D. G.
12 H., Jackson, D. R., Polavarapu, S., Compo, G. P., Dragani, R., Ebisuzaki, W., Harada, Y., Kobayashi,
13 C., McCarty, W., Onogi, K., Pawson, S., Simmons, A., Wargan, K., Whitaker, J. S., and Zou, C.-Z.:
14 Introduction to the SPARC Reanalysis Intercomparison Project (S-RIP) and overview of the reanalysis
15 systems, *Atmos. Chem. Phys.*, 17, 1417-1452, <https://doi.org/10.5194/acp-17-1417-2017>, 2017.
- 16 Gelaro, R., W. McCarty, M.J. Suárez, R. Todling, A. Molod, L. Takacs, C.A. Randles, A. Darmenov,
17 M.G. Bosilovich, R. Reichle, K. Wargan, L. Coy, R. Cullather, C. Draper, S. Akella, V. Buchard, A.
18 Conaty, A.M. da Silva, W. Gu, G. Kim, R. Koster, R. Lucchesi, D. Merkova, J.E. Nielsen, G. Partyka,
19 S. Pawson, W. Putman, M. Rienecker, S.D. Schubert, M. Sienkiewicz, and B. Zhao: The Modern-Era
20 Retrospective Analysis for Research and Applications, Version 2 (MERRA-2). *J. Climate*, 30, 5419–
21 5454, <https://doi.org/10.1175/JCLI-D-16-0758.1>, 2017.
- 22 Gettelman, A., M. L. Salby, and F. Sassi: Distribution and influence of convection in the tropical
23 tropopause region. *J. Geophys. Res.*, 107, 4080, doi:10.1029/2001JD001048, 2002.
- 24 Gettelman, A., et al., Multimodel assessment of the upper troposphere and lower stratosphere: Tropics
25 and global trends, *J. Geophys. Res.*, 115, D00M08, doi:10.1029/2009JD013638, 2010.
- 26 Global Modeling and Assimilation Office (GMAO), MERRA-2 inst6_3d_ana_Nv: 3d,6-Hourly,
27 Instantaneous, Model-Level, Analysis, Analyzed Meteorological Fields V5.12.4, Greenbelt, MD, USA,
28 Goddard Earth Sciences Data and Information Services Center (GES DISC), Accessed: [1.1.2015],
29 10.5067/IUUF4WB9FT4W, 2015.
- 30 Gorbunov, M. E., Benzon, H.-H., Jensen, A. S., Lohmann, M. S., and Nielsen, A. S.: Comparative
31 analysis of radio occultation processing approaches based on Fourier integral operators, *Radio Science*,
32 39, RS6004, <https://doi.org/10.1029/2003RS002916>, 2004.
- 33 Haimberger, L., Homogenization of Radiosonde Temperature Time Series Using Innovation Statistics.
34 *J. Climate*, 20, 1377–1403, <https://doi.org/10.1175/JCLI4050.1>, 2007.
- 35 Haimberger, L., Tavolato, C., and Sperka, S.: Homogenization of the Global Radiosonde Temperature
36 Dataset through Combined Comparison with Reanalysis Background Series and Neighboring Stations,
37 *J. Climate*, 25, 8108–8131, <https://doi.org/10.1175/JCLI-D-11-00668.1>, 2012.
- 38 Hajj, G. A., Ao, C. O., Iijima, B. A., Kuang, D., Kursinski, E. R., Mannucci, A. J., Meehan, T. K.,
39 Romans, L. J., de la Torre Juarez, M., and Yunck, T. P.: CHAMP and SAC-C atmospheric occultation
40 results and intercomparisons, *Journal of Geophysical Research (Atmospheres)*, 109, D06 109,
41 <https://doi.org/10.1029/2003JD003909>, 2004.

1 Hartmann, D. L., J. R. Holton, and Q. Fu: The heat balance of the tropical tropopause, cirrus, and
2 stratospheric dehydration. *Geophys. Res. Lett.*, 28, 1969–1972, 2001

3 Hersbach, H., et al., Operational global reanalysis: progress, future directions and synergies with NWP,
4 ERA Report Series, 27, 2018.

5 Highwood, E. J. and Hoskins, B. J., The tropical tropopause. *Q.J.R. Meteorol. Soc.*, 124: 1579-1604.
6 doi:10.1002/qj.49712454911, 1998.

7 Ho, S.-p., Peng, L., and Vömel, H.: Characterization of the longterm radiosonde temperature biases in
8 the upper troposphere and lower stratosphere using COSMIC and Metop-A/GRAS data from 2006 to
9 2014, *Atmospheric Chemistry & Physics*, 17, 4493–4511, <https://doi.org/10.5194/acp-17-4493-2017>,
10 2017.

11 Holton, J. R. and Gettelman, A.: Horizontal transport and the dehydration of the stratosphere, *Geophys.*
12 *Res. Lett.*, 28, 2799–2802, 2001.

13 Kim, J. and S. Son: Tropical Cold-Point Tropopause: Climatology, Seasonal Cycle, and Intraseasonal
14 Variability Derived from COSMIC GPS Radio Occultation Measurements. *J. Climate*, 25, 5343–5360,
15 <https://doi.org/10.1175/JCLI-D-11-00554.1>, 2012.

16 Kim, Y.-H., Kiladis, G. N., Albers, J. R., Dias, J., Fujiwara, M., Anstey, J. A., Song, I.-S., Wright, C.
17 J., Kawatani, Y., Lott, F., and Yoo, C.: Comparison of equatorial wave activity in the tropical tropopause
18 layer and stratosphere represented in reanalyses, *Atmos. Chem. Phys. Discuss.*,
19 <https://doi.org/10.5194/acp-2019-110>, in review, 2019.

20 Kistler, R., Collins, W., Saha, S., White, G., Woollen, J., Kalnay, E., Chelliah, M., Ebisuzaki, W., Kanamitsu,
21 M., Kousky, V., van den Dool, H., Jenne, R., and Fiorino, M.: The NCEP–NCAR 50-year reanalysis: monthly
22 means CD-ROM and documentation, *B. Am. Meteorol. Soc.*, 82, 247–267, 2001.

23 Kobayashi, S., Ota, Y., Harada, Y., Ebata, A., Moriya, M., Onoda, H., Onogi, K., Kamahori, H.,
24 Kobayashi, C., Endo, H., Miyaoka, K., and Takahashi, K.: The JRA-55 reanalysis: general specifica-
25 tions and basic characteristics, *J. Meteorol. Soc. Jpn.*, 93, 5–48, doi:10.2151/jmsj.2015-001, 2015.

26 Krüger, K., Tegtmeier, S., and Rex, M.: Long-term climatology of air mass transport through the
27 Tropical Tropopause Layer (TTL) during NH winter, *Atmos. Chem. Phys.*, 8, 813-823,
28 <https://doi.org/10.5194/acp-8-813-2008>, 2008.

29 Krüger, K., Tegtmeier, S., and Rex, M.: Variability of residence time in the Tropical Tropopause Layer
30 during Northern Hemisphere winter, *Atmos. Chem. Phys.*, 9, 6717-6725, <https://doi.org/10.5194/acp-9-6717-2009>, 2009.

32 Kursinski, E. R., Hajj, G. A., Schofield, J. T., Linfield, R. P., and Hardy, K. R.: Observing Earth’s
33 atmosphere with radio occultation measurements using the Global Positioning System, *Journal of*
34 *Geophysical Research: Atmospheres*, 102, 23 429–23 465, <https://doi.org/10.1029/97JD01569>, 1997.

35 Lawrence, Z. D., Manney, G. L., and Wargan, K.: Reanalysis intercomparisons of stratospheric polar
36 processing diagnostics, *Atmos. Chem. Phys.*, 18, 13547-13579, [https://doi.org/10.5194/acp-18-13547-](https://doi.org/10.5194/acp-18-13547-2018)
37 2018, 2018.

38 Long, C. S., Fujiwara, M., Davis, S., Mitchell, D. M., and Wright, C. J.: Climatology and interannual
39 variability of dynamic variables in multiple reanalyses evaluated by the SPARC Reanalysis

- 1 Intercomparison Project (S-RIP), *Atmos. Chem. Phys.*, 17, 14593-14629, [https://doi.org/10.5194/acp-](https://doi.org/10.5194/acp-17-14593-2017)
2 17-14593-2017, 2017.
- 3 Maycock, A.C., et al., Revisiting the mystery of stratospheric temperature trends. *Geophys. Res. Lett.*,
4 doi:10.1029/2018GL078035, 2018.
- 5 Mote, P. W., Rosenlof, K. H., McIntyre, M. E., Carr, E. S., Gille, J. C., Holton, J. R., Kinnnersley, J. S.,
6 Pumphrey, H. C., Russell, J. M., and Waters, J. W.: An atmospheric tape recorder: The imprint of
7 tropical tropopause temperatures on stratospheric water vapor, *J. Geophys. Res.*, 101(D2), 3989–4006,
8 doi:10.1029/95JD03422, 1996.
- 9 Nash, J., Oakley, T., Vömel, H., and Li, W.: WMO intercomparison of high-quality radiosonde systems,
10 Yangjiang, China, 12 July–3 August 2010, Instruments and Observing Methods Re- port No. 107,
11 WMO/TD-No. 1580, WMO, Geneva, Switzerland, 238 pp., 2011.
- 12 Naujokat, B., An update of the observed quasi-biennial oscillation of the stratospheric winds over the tropics,
13 *J. Atmos. Sci.*, 43, 1873-1877, 1986.
- 14 Nishimoto, E., and M. Shiotani, Seasonal and interannual variability in the temperature structure around
15 the tropical tropopause and its relationship with convective activities, *J. Geophys. Res. Atmos.*, 117,
16 D02104, doi:10.1029/2011JD016936, 2012.
- 17 Nishimoto, E., and M. Shiotani, Intraseasonal variations in the tropical tropopause temperature revealed
18 by cluster analysis of convective activity, *J. Geophys. Res. Atmos.*, 118, 3545–3556, doi:
19 10.1002/jgrd.50281, 2013.
- 20 Onogi, K., Tsutsui, J., Koide, H., Sakamoto, M., Kobayashi, S., Hat-
21 sushika, H., Matsumoto, T., Yamazaki, N., Kamahori, H., Taka-
22 hashi, K., Kadokura, S., Wada, K., Kato, K., Oyama, R., Ose, T.,
23 Mannoji, N., and Taira, R.: The JRA-25 reanalysis, *J. Meteorol. Soc. Jpn.*, 85, 369–432,
doi:10.2151/jmsj.85.369, 2007.
- 24 Pan, L. L., and Munchak, L. A.: Relationship of cloud top to the tropopause and jet structure from
25 CALIPSO data, *J. Geophys. Res.*, 116, D12201, doi:10.1029/2010JD015462, 2011.
- 26 Pan, L. L., Honomichl, S. B., Bui, T. V., Thornberry, T., Rollins, A., Hints, E., & Jensen, E. J.: Lapse
27 Rate or Cold Point: The Tropical Tropopause Identified by In Situ Trace Gas Measurements.
28 *Geophysical Research Letters*, 45(19), 10-756, 2018.
- 29 Randel W. J., and Jensen, E., Physical processes in the tropical tropopause layer and their roles in a
30 changing climate. *Nat Geosci* 6:169–176, 2013.
- 31 Randel, W. J., F. Wu, and D. J. Gaffen, Low frequency variations of the tropical tropopause from NCEP
32 reanalyses. *J. Geophys. Res.*, 105, 15 509–15 523, 2000.
- 33 Randel, W. J., F. Wu, S.J. Oltmans, K. Rosenlof, and G.E. Nedoluha, Interannual Changes of
34 Stratospheric Water Vapor and Correlations with Tropical Tropopause Temperatures. *J. Atmos. Sci.*,
35 61, 2133–2148, <https://doi.org/10.1175/1520-0469>, 2004a.
- 36 Randel, W. J., P. Udelhofen, E. Fleming, M. Geller, M. Gelman, K. Hamilton, D. Karoly, D. Ortland,
37 S. Pawson, R. Swinbank, F. Wu, M. Baldwin, M. Chanin, P. Keckhut, K. Labitzke, E. Remsberg, A.
38 Simmons, and D. Wu, The SPARC Intercomparison of Middle-Atmosphere Climatologies. *J. Climate*,
39 17, 986–1003, [https://doi.org/10.1175/1520-0442\(2004\)017](https://doi.org/10.1175/1520-0442(2004)017), 2004b.

- 1 Randel, W. J., Shine, K. P., Austin, J., Barnett, J., Claud, C., Gillett, N. P., et al., An update of observed
2 stratospheric temperature trends. *Journal of Geophysical Research*, 114, D02107.
3 <https://doi.org/10.1029/2008JD010421>, 2009.
- 4 Rienecker, M. M., Suarez, M. J., Gelaro, R., Todling, R., Bacmeister, J., Liu, E., Bosilovich, M. G.,
5 Schubert, S. D., Takacs, L., Kim, G.-K., Bloom, S., Chen, J., Collins, D., Conaty, A., da Silva, A., Gu,
6 W., Joiner, J., Koster, R. D., Lucchesi, R., Molod, A., Owens, T., Pawson, S., Pegion, P., Redder, C. R.,
7 Reichle, R., Robertson, F. R., Ruddick, A. G., Sienkiewicz, M., and Woollen, J.: MERRA: NASA's
8 modern-era retrospective analysis for research and applications, *J. Climate*, 24, 3624–3648,
9 doi:10.1175/JCLI-D-11-00015.1, 2011.
- 10 Saha, S., Moorthi, S., Pan, H.-L., Wu, X., Wang, J., Nadiga, S., Tripp, P., Kistler, R., Woollen, J.,
11 Behringer, D., Liu, H., Stokes, D., Grumbine, R., Gayno, G., Wang, J., Hou, Y.-T., Chuang, H.-Y.,
12 Juang, H.-M. H., Sela, J., Iredell, M., Treadon, R., Kleist, D., van Delst, P., Keyser, D., Derber, J., Ek,
13 M., Meng, J., Wei, H., Yang, R., Lord, S., van den Dool, H., Kumar, A., Wang, W., Long, C., Chelliah,
14 M., Xue, Y., Huang, B., Schemm, J.-K., Ebisuzaki, W., Lin, R., Xie, P., Chen, M., Zhou, S., Higgins,
15 W., Zou, C.-Z., Liu, Q., Chen, Y., Han, Y., Cucurull, L., Reynolds, R. W., Rutledge, G., and Goldberg,
16 M.: The NCEP climate forecast system reanalysis, *B. Am. Meteorol. Soc.*, 91, 1015–1057,
17 doi:10.1175/2010BAMS3001.1, 2010.
- 18 Santer, B.D., R. Sausen, T.M.L. Wigley, J.S. Boyle, K. AchutaRao, C. Doutriaux, J.E. Hansen, G.A.
19 Meehl, E. Roeckner, R. Ruedy, G. Schmidt, and K.E. Taylor, Behavior of tropopause height and
20 atmospheric temperature in models, reanalyses, and observations: Decadal changes. *J. Geophys. Res.*,
21 108, no. D1, 4002, doi:10.1029/2002JD002258, 2003.
- 22 Schoeberl, M. R., A. E. Dessler, and T. Wang., Simulation of stratospheric water vapor and trends using
23 three reanalyses." *Atmospheric Chemistry and Physics*, 12 (14): 6475-6487 doi:10.5194/acp-12-6475-
24 2012, 2012.
- 25 Seidel, D. J., and Randel, W. J., Variability and trends in the global tropopause estimated from
26 radiosonde data, *J. Geophys. Res.*, 111, D21101, doi:10.1029/2006JD007363, 2006
- 27 Seidel, D. J., R. J. Ross, J. K. Angell, and G. C. Reid, Climatological characteristics of the tropical
28 tropopause as revealed by radiosondes, *J. Geophys. Res.*, 106(D8), 7857–7878,
29 doi:10.1029/2000JD900837, 2001.
- 30 Sherwood, S. C., T. Horinouchi, and H. A. Zeleznik: Convective impact on temperatures observed near
31 the tropical tropopause. *J. Atmos. Sci.*, 60, 1847–1856, 2003.
- 32 Simmons, A. J., Poli, P., Dee, D. P., Berrisford, P., Hersbach, H., Kobayashi, S. and Peubey, C.,
33 Estimating low-frequency variability and trends in atmospheric temperature using ERA-Interim. *Q.J.R.*
34 *Meteorol. Soc.*, 140: 329-353. doi:10.1002/qj.2317, 2014.
- 35 Tao, M., Konopka, P., Ploeger, F., Yan, X., Wright, J. S., Diallo, M., Fueglistaler, S., and Riese, M.:
36 Multitimescale variations in modeled stratospheric water vapor derived from three modern reanalysis
37 products, *Atmos. Chem. Phys.*, 19, 6509–6534, <https://doi.org/10.5194/acp-19-6509-2019>, 2019.
- 38 Thorne, P. W., D. E. Parker, S. F. B. Tett, P. D. Jones, M. McCarthy, H. Coleman, and P. Brohan,
39 Revisiting radiosonde upper air temperatures from 1958 to 2002, *J. Geophys. Res.*, 110, D18105,
40 doi:10.1029/2004JD005753, 2005.

1 Thomason, L. W., Ernest, N., Millán, L., Rieger, L., Bourassa, A., Vernier, J.-P., Manney, G., Luo, B.,
2 Arfeuille, F., and Peter, T.: A global space-based stratospheric aerosol climatology: 1979–2016, *Earth*
3 *Syst. Sci. Data*, 10, 469–492, <https://doi.org/10.5194/essd-10-469-2018>, 2018.

4 von Engel, A., Andres, Y., Marquardt, C., and Sancho, F.: GRAS radio occultation on-board of Metop,
5 *Advances in Space Research*, 47, 336–347, <https://doi.org/10.1016/j.asr.2010.07.028>, 2011.

6 Wang, J. S., Seidel, D. J., and Free, M., How well do we know recent climate trends at the tropical
7 tropopause?, *J. Geophys. Res.*, 117, D09118, doi:10.1029/2012JD017444, 2012.

8 Wheeler, M. and G.N. Kiladis, Convectively Coupled Equatorial Waves: Analysis of Clouds and
9 Temperature in the Wavenumber–Frequency Domain. *J. Atmos. Sci.*, 56, 374–399,
10 [https://doi.org/10.1175/1520-0469\(1999\)056<0374:CCEWAO>2.0.CO;2](https://doi.org/10.1175/1520-0469(1999)056<0374:CCEWAO>2.0.CO;2), 1999.

11 Wickert, J., Reigber, C., Beyerle, G., König, R., Marquardt, C., Schmidt, T., Grunwaldt, L., Galas, R.,
12 Meehan, T. K., Melbourne, W. G., and Hocke, K.: Atmosphere sounding by GPS radio occultation: First
13 results from CHAMP, *Geophysical Research Letters*, 28, 3263–3266,
14 <https://doi.org/10.1029/2001GL013117>, 2001.

15 World Meteorological Organization: Definition of the tropopause, *Bulletin of the World Meteorological*
16 *Organization*, 6, 136–137, 1957.

17 Wright, C. J. and Hindley, N. P.: How well do stratospheric reanalyses reproduce high-resolution satellite
18 temperature measurements?, *Atmos. Chem. Phys.*, 18, 13703–13731, [https://doi.org/10.5194/acp-18-](https://doi.org/10.5194/acp-18-13703-2018)
19 [13703-2018](https://doi.org/10.5194/acp-18-13703-2018), 2018.

20 Xie, F., Li, J., Tian, W., Li, Y., & Feng, J., Indo-Pacific warm pool area expansion, Modoki activity,
21 and tropical cold-point tropopause temperature variations. *Scientific reports*, 4, 4552.
22 doi:10.1038/srep04552, 2014.

23 Zhou, X.L., M.A. Geller, and M.H. Zhang, Tropical Cold Point Tropopause Characteristics Derived
24 from ECMWF Reanalyses and Soundings. *J. Climate*, 14, 1823–1838, [https://doi.org/10.1175/1520-](https://doi.org/10.1175/1520-0442(2001)14<1823:TCPTRP>2.0.CO;2)
25 [0442\(2001\)14<1823:TCPTRP>2.0.CO;2](https://doi.org/10.1175/1520-0442(2001)14<1823:TCPTRP>2.0.CO;2), 2001.

26

27